

Stacked generalization ensemble learning strategy for multivariate prediction of delamination and maximum thrust force in composite drilling

Baraheni, Mohammad; Soudmand, Behzad Hashemi; Amini, Saeid; Fotouhi, Mohammad

DOI

[10.1177/00219983241289494](https://doi.org/10.1177/00219983241289494)

Publication date

2024

Document Version

Final published version

Published in

Journal of Composite Materials

Citation (APA)

Baraheni, M., Soudmand, B. H., Amini, S., & Fotouhi, M. (2024). Stacked generalization ensemble learning strategy for multivariate prediction of delamination and maximum thrust force in composite drilling. *Journal of Composite Materials*, 58(30), 3113-3138. <https://doi.org/10.1177/00219983241289494>

Important note

To cite this publication, please use the final published version (if applicable). Please check the document version above.

Copyright

Other than for strictly personal use, it is not permitted to download, forward or distribute the text or part of it, without the consent of the author(s) and/or copyright holder(s), unless the work is under an open content license such as Creative Commons.

Takedown policy

Please contact us and provide details if you believe this document breaches copyrights. We will remove access to the work immediately and investigate your claim.

Green Open Access added to TU Delft Institutional Repository

'You share, we take care!' - Taverne project

<https://www.openaccess.nl/en/you-share-we-take-care>

Otherwise as indicated in the copyright section: the publisher is the copyright holder of this work and the author uses the Dutch legislation to make this work public.

Stacked generalization ensemble learning strategy for multivariate prediction of delamination and maximum thrust force in composite drilling

Journal of Composite Materials
2024, Vol. 58(30) 3113–3138
© The Author(s) 2024
Article reuse guidelines:
sagepub.com/journals-permissions
DOI: 10.1177/00219983241289494
journals.sagepub.com/home/jcm


Mohammad Baraheni¹ , Behzad Hashemi Soudmand², Saeid Amini³  and Mohammad Fotouhi⁴ 

Abstract

The complexity of drilling carbon fiber reinforced polymers (CFRP) requires accurate predictive models. This study addresses the challenge using an ensemble machine learning (ML) approach with stacked generalization. The model captures the relationships between key input variables—such as graphene nanoplatelet (GNP) content, ultrasonic assistance, tool type, stacking sequence, and feed rate—and output parameters, specifically thrust force and delamination. A nested feature scoring (NFS) method was employed for importance analysis, revealing tooling type and feed rate as key features for minimizing delamination and reducing thrust force, respectively. The machinability results revealed that ultrasonic drilling lowered thrust force by improving chip evacuation and reducing fiber breakage. HSS tools with cobalt content, alongside symmetrical stacking sequence, helped to further minimize both thrust force and delamination. However, the inclusion of GNPs led to an increase in thrust force and delamination, attributed to the increased strength of the CFRP/GNP composite. The process involved meticulous training, resulting in four optimal-fit models serving as inputs for the stacked meta-model. Iterative enhancements fortified the ensemble robustness, with fine-tuning of hyperparameters through Bayesian optimization. The ensemble superiority over individual models manifested in a remarkable reduction of mean absolute error (MAE) and root mean squared error (RMSE) by up to 97% and 124% for delamination, and 205% and 154% for thrust force, compared to the best base learner. Visual and statistical assessments effectively illuminated the intricate interactions between variables in the drilling process. The methodology resulted in a highly adaptable predictive model with applications across diverse manufacturing contexts.

Keywords

Composite drilling, delamination, stacked generalization scheme, multivariate machine learning, feature importance analysis

Introduction

Carbon fiber reinforced polymers (CFRP) have emerged as pioneering materials, providing sophisticated applications due to their remarkable strength-to-weight ratio.^{1–4} The significant characteristic of CFRPs lies in the exceptional load-bearing capacity attributed to the carbon fibers, which account for up to 80% of the overall strength.⁵ To ensure the desired surface integrity of CFRP for structural applications, it is crucial to carefully select and optimize the structural and machining parameters during fabrication. Among fabrication techniques, drilling is a widely used secondary machining process for assembling parts and joining fiber-reinforced composites.^{6,7} Drilling CFRP composites is followed by challenges due to their heterogeneous and

¹Department of Manufacturing, Faculty of Mechanical Engineering, Arak University of Technology, Arak, Iran

²Department of Mechanical Engineering, Gebze Technical University, Kocaeli, Turkiye

³Department of Manufacturing, Faculty of Mechanical Engineering, University of Kashan, Kashan, Iran

⁴Faculty of Materials, Mechanics, Management & Design (3MD), Delft University of Technology, Delft, the Netherlands

Corresponding author:

Mohammad Baraheni, Department of Manufacturing, Faculty of Mechanical Engineering, Arak University of Technology, Daneshgah street, Arak 3818146763, Iran.

Email: mbaraheni@arakut.ac.ir

Data Availability Statement included at the end of the article

anisotropic nature, resulting in delamination, fiber pull-out, fuzzing, and matrix smearing, which can in turn deteriorate the part quality and lower its service life.⁸ The integration of nanofillers into composite materials significantly enhances their properties due to the substantial surface contact these fillers provide with the host matrix, even at low inclusion levels.^{9–12} This enhancement broadens the range of applications by allowing the tailoring of nanocomposites to meet specific performance requirements.^{13–15} Various types of nanoparticles have been utilized to improve the reinforcement of laminated composites, including graphene nanoplatelets (GNPs),^{16–18} nano calcium carbonate,^{1,3} carbon nano-onions,¹⁹ and multi-walled carbon nanotubes,²⁰ among others.

Delamination is a frequent and problematic defect in composite drilling, impacting fatigue endurance and surface integrity.²¹ It arises from two distinct mechanisms: push-out and peel-up, based on the workpiece entrance and exit planes.²² Push-out delamination is more common than peel-up delamination due to improper material support caused by excessive thrust force, which weakens intralaminar adhesion strength and promotes crack growth.²³ The factors contributing to this type of delamination can be classified into two main categories: machining parameters such as feed rate, torque, and spindle speed and structural properties like stacking sequence and constituent phases.²⁴ Dubey et al.²⁵ demonstrated that a stacking sequence comprising four layers each of glass and carbon fibers yielded an optimal balance, with a thrust force of 59.05 N and a delamination factor of 1.001. Similarly, Kumar et al.²⁶ optimized milling parameters to reduce delamination in laminated nanocomposites, identifying the feed rate as the most significant factor, contributing 62.60% to the overall effect. In addition, various criteria for evaluating delamination were suggested, with the key factors outlined in Table 1.

Various factors influence delamination during the drilling of composites. Employing specialized drill bits, such as

saw, candlestick, and core drills, along with techniques like step drilling, pilot holes, and the use of back-up plates, was shown to effectively reduce thrust force and mitigate delamination.³⁴ Rahme et al.³⁵ experimentally and analytically demonstrated that step gun drills are particularly effective in minimizing delamination at the hole exit. In another study, Rahme et al.³⁶ found that incorporating a woven glass ply at the hole exit can significantly reduce delamination and improve structural integrity. Furthermore, non-traditional methods like waterjet, ultrasonic machining, and laser cutting offer unique benefits, though they often come with trade-offs, such as higher costs or slower production speeds. Vibration-assisted drilling was also proven to improve traditional drilling methods when applied with proper control.³⁴

The complexity arising from a large number of input control factors and constraints on conducting experimental tests to explore optimal cutting conditions and enhance surface integrity highlights the need for cognitive computing strategies. These approaches can effectively model the drilling process and reveal intricate relationships between the influential input parameters and the desired targets. In this regard, soft computing techniques, such as response surface methodology (RSM), Fuzzy design principles, artificial neural networks (ANN), and metaheuristic approaches were utilized in literature as alternatives to traditional statistical methods for analyzing drilling processes of CFRP composites.^{37–41} Kumar et al.⁴² employed an integrated methodology combining Grey relational analysis (GRA) and principal component analysis (PCA) within the framework of the technique for order of preference by similarity to ideal solution (TOPSIS) to optimize milling outcomes, specifically surface roughness and cutting force. Similarly, Kesrawani et al.⁴³ applied GRA and GRA-PCA techniques to optimize the machining parameters for hybrid MWCNT/GFRP nanocomposites, achieving a 4.935% efficiency enhancement using the Taguchi method. Kumar et al.⁴⁴ employed simulated annealing (SA)

Table 1. Frequently used delamination factors for evaluating delamination.

Correlation	Source	Correlation description
$F_d = \frac{D_{max}}{D}$	Chen et al. ²⁷	D_{max} : Maximum delamination diameter; D : Nominal drilled hole diameter
$F_a = \left(\frac{A_d}{A_{nom}}\right) \times 100$	Faraz et al. ²⁸	A_d : Total damaged area; A_{nom} : Nominal drill area
$D_{RAT} = \frac{D_{MAR}}{A_{AVG}}$	Mehta et al. ²⁹	D_{MAR} : Damaged area at hole periphery; A_{AVG} : Average nominal drilled hole area
$F_{da} = \alpha \frac{D_{max}}{D_0} + \beta \frac{A_{max}}{A_0}$	Davim et al. ³⁰	α and β are weights where $\alpha = 1 - \beta$; β is the ratio of $A_d = \frac{A_d}{(A_{max} - A_0)}$, with A_d being the damaged area, A_{max} the area for D_{max} ; and A_0 the area for D_0
$F_{ed} = \frac{D_e}{D_0}$	Tsao et al. ³¹	$D_e = \left(\frac{4(A_d + A_0)}{\pi}\right)^{0.5}$, where A_d is the damaged area and A_0 is the nominal area
$f = 4\pi \frac{A}{P^2}$	Durao et al. ³²	A : Damaged area; P : Perimeter of the damaged area
$F_{dmin} = \frac{D_{min}}{D_0}$	Silva et al. ³³	D_{min} : Minimum diameter enclosing the damaged area; D_0 : Nominal drilled hole area

algorithm to optimize delamination in Graphene oxide (GO)-reinforced CFRP nanocomposites. The input variables encompassed GO loading, spindle speed, and feed rate. Validation was performed through a confirmatory test, demonstrating favorable agreement with actual results. The study highlighted the significant influence of feed rate on delamination and thrust, followed by GO concentration. Vijayan et al.⁴⁵ utilized an integrated approach involving RSM and particle swarm optimization (PSO) to enhance the drilling performance of CFRP- carbon nanotube (CNT) nanocomposites. Kumar et al.⁴⁶ investigated the drilling behavior of GO-reinforced CFRPs using a hybrid approach of GRA-PCA to determine the optimal drilling process parameters. Kaybal et al.⁴⁷ utilized RSM to optimize delamination factor and thrust force in drilling of CNT-included CFRP composites, by employing Lagrange multipliers and Kuhn-Tucker conditions. Shetty et al.⁴⁸ introduced a genetic algorithm optimized multi-layer perceptron neural network (GA-MLPNN) prediction framework to model and subsequently optimize thrust force in the drilling of CFRP. They also compared the optimization outcomes and those obtained from RSM model and the results demonstrated the superiority of the GA-MLPNN model over RSM in terms of predictive accuracy. Panchagnula et al.⁴⁹ employed two deep neural networks (DNNs) to predict delamination circularity deviation in glass fiber-reinforced polymers (GFRPs) reinforced with multi-walled carbon nanotubes (MWCNT). Ge et al.⁵⁰ combined non-dominated sorting genetic algorithm (NSGA-II) and TOPSIS to effectively rank the resulting pareto front and thus identify the optimal solution for optimizing the CFRP drilling process. Soepangkat et al.⁵¹ employed an integrated back propagation neural network (BPNN)-PSO algorithm to model the drilling process and attain optimal responses in the drilling process of CFRP.

Various data-centric methods were examined for modeling and optimizing the drilling process, focusing on factors like tooling, nano-reinforcements, and machining parameters. Machine learning (ML) algorithms have shown promise for improving complex processes across different fields. Recent research often uses artificial ANNs, either alone or combined with response surface methods or optimization algorithms. Despite their advantages in accurate non-linear fitting and predictions, ANNs have some drawbacks: they depend on initial random weight settings, lack interpretability, may face convergence issues with backpropagation, and can suffer from overfitting, affecting generalization.⁵² As an alternative, decision trees provide benefits such as faster training, easier hyperparameter tuning, better interpretability, and improved generalization.⁵³

Due to the limitations of single ML models, ensemble learning methods have become more popular. These methods combine multiple base learners to achieve high

accuracy and improved stability compared to individual models.⁵⁴ In this study, a tree-based ensemble technique was used for modeling CFRP composite drilling operations, employing a second-level meta-model. The stacking method was chosen for its ability to integrate various models into a single, robust model. Stacking involves training multiple base models and then combining them into a meta-model to enhance prediction accuracy and reliability.⁵⁵

To overcome the limitations of individual ML models with small datasets, ensemble techniques can be used to combine multiple learners. Ensemble learning improves the robustness and generalization of predictive models by aggregating the predictions of several base estimators. This method enhances performance and resilience against data variations compared to using a single model.⁵² Ensembles can be either homogeneous, using models from the same algorithm, or heterogeneous, combining models from different algorithms.⁵⁶ Common ensemble approaches include bagging, boosting, and stacking.

The bagging algorithm is a fundamental ensemble machine learning method suited for datasets with limited training samples. It improves regression and classification accuracy by combining predictions from multiple models, each with different classifiers, features, and parameters. This approach is particularly effective for models with high variance. By averaging predictions from diverse models, the method reduces the impact of individual errors, leading to more accurate forecasts. The effectiveness of the ensemble depends on the level of error correlation among the models, with lower correlation typically resulting in better overall accuracy.⁵⁷

Boosting, as an ensemble technique, enhances the accuracy and effectiveness of machine learning algorithms by iteratively introducing new learners to improve the performance of weaker models. It helps address overfitting issues often associated with decision trees, leading to models with reduced variance and bias. Boosting involves creating multiple training datasets through random sampling with replacement, similar to bagging. The process begins with training the first model on the initial dataset, and subsequent models refine the predictions of the earlier ones. The final robust model is constructed by combining all weak learners through averaging or weighted majority voting.⁵⁸

The use of ensemble ML techniques in CFRP drilling has recently garnered interest due to their capability to enhance predictive accuracy and handle complex interactions among variables. Techniques such as bagging-based methods, including Random Forest (RF), and boosting approaches like Gradient Boosting, were applied to predict critical outcomes in drilling processes. For example, Nargis et al.⁵⁹ explored the use of ANN and RF for predictive analysis of drilling performance in CFRP and hybrid nano-composites,

highlighting RF superior accuracy over ANN and traditional statistical methods like response RSM. Similarly, Guo et al.⁶⁰ applied the extreme gradient boosting algorithm (XGBoost) to predict the impact of milling parameters on CFRP strength, revealing XGBoost enhanced performance compared to ANN. Despite the high potential of ensemble machine learning techniques in advancing the precision and efficiency of CFRP machining processes, very limited bodies of scholar were conducted in this field.

Stacking, a meta-learning technique, improves predictive accuracy by combining predictions from multiple base models. This method involves training a meta-model to integrate the predictions from various base learners, aiming to reduce generalization errors and enhance the final ensemble model's performance. The process consists of two main steps: First, multiple first-level models are trained on the dataset, and their predictions are collected to form a new dataset, where each instance is labeled with the true value it predicts. In the second step, this new dataset is used with a meta-learning algorithm to produce the final output (see⁶¹). The out-of-fold predictions from the base models are employed to train the second-level meta-learner, leading to the final ensemble prediction.

While ML techniques were extensively utilized to develop predictive models for the drilling of CRFP, a research gap exists in the literature regarding the application of ensemble ML methods within this specific context. The stacking approach involves the utilization of a variety of models to create a comprehensive data learning model. In this context, a diverse range of base learners, including both ensemble tree-based and non-ensemble predictors, were assessed, and the most suitable candidates were selected as inputs for the meta-model. The dataset was generated through a design of experiments (DoE) using Taguchi methodology. The meta-learner chosen was stochastic gradient boosting regression (SGBR), and its hyperparameters were fine-tuned using Bayesian optimization. The categorical input variables encompassed stacking sequence, ultrasonics status (non-ultrasonic or ultrasonic-induced process), material type (with and without GNP), and drill type, while feed rate (0.08, 0.15, and 0.25 mm/rev)

was the sole continuous feature. The developed model aimed to predict delamination and thrust force as desired outcomes. Moreover, a novel nested method for ranking feature importance was introduced to gauge the significance of features and sub-features in terms of their impact on the target responses. Furthermore, a combination of visual experimentation and statistical methodologies was employed to assess both the qualitative and quantitative influence of the input variables on delamination and thrust force. The findings presented in this study offer a systematic approach for comparing different ML techniques concerning their efficacy in predicting delamination and thrust force in CRFP drilling.

Materials and methods

Material specifications

The samples were fabricated using ML506 epoxy resin, characterized by a viscosity of 1450 cP at 25°C,⁶² and reinforced with T700 unidirectional carbon fibers and GNP. The hand-layup technique was employed to produce plate-shaped composites, each measuring 200 × 200 mm with a thickness of 2 mm. A total of eight plies were layered to form the plates, following a stacking sequence of (0₂, 90₂), arranged in both symmetrical and asymmetrical configurations. After the layers were assembled, the plates underwent a controlled curing process to ensure optimal bonding and material consolidation. Two types of specimens were considered: pristine CFRP and hybrid CFRP-GNP. The GNP loading was 0.25 wt%, selected based on a previous research findings as the threshold for agglomeration.⁶³ Table 2 presents the properties of the nanoparticles, carbon fibers, and epoxy resin used in the study.

Experimental layout

The drilling tools used in this investigation included high-speed steel (HSS), and HSS containing 5% (HSS-5% Co) and 8% Cobalt (HSS-8% Co), as illustrated in Figure 1(a). Experimental tests were carried out using a

Table 2. Specifications of the constituent materials.

Property	Epoxy ML506	T700 carbon fiber	GNP	Unit
Density	1.11	1.8	-	gr/cm ³
Tensile strength	75	3800	-	MPa
Tensile modulus	2.82	210	-	GPa
Coefficient of thermal expansion	12 × 10 ⁻⁶	0.15 × 10 ⁻⁵	-	1/°C
Thickness	-	0.2	<60	mm
Purity	-	-	98.5	%
Surface area	-	-	40	m ² /gr
Lateral size	-	-	7	μm

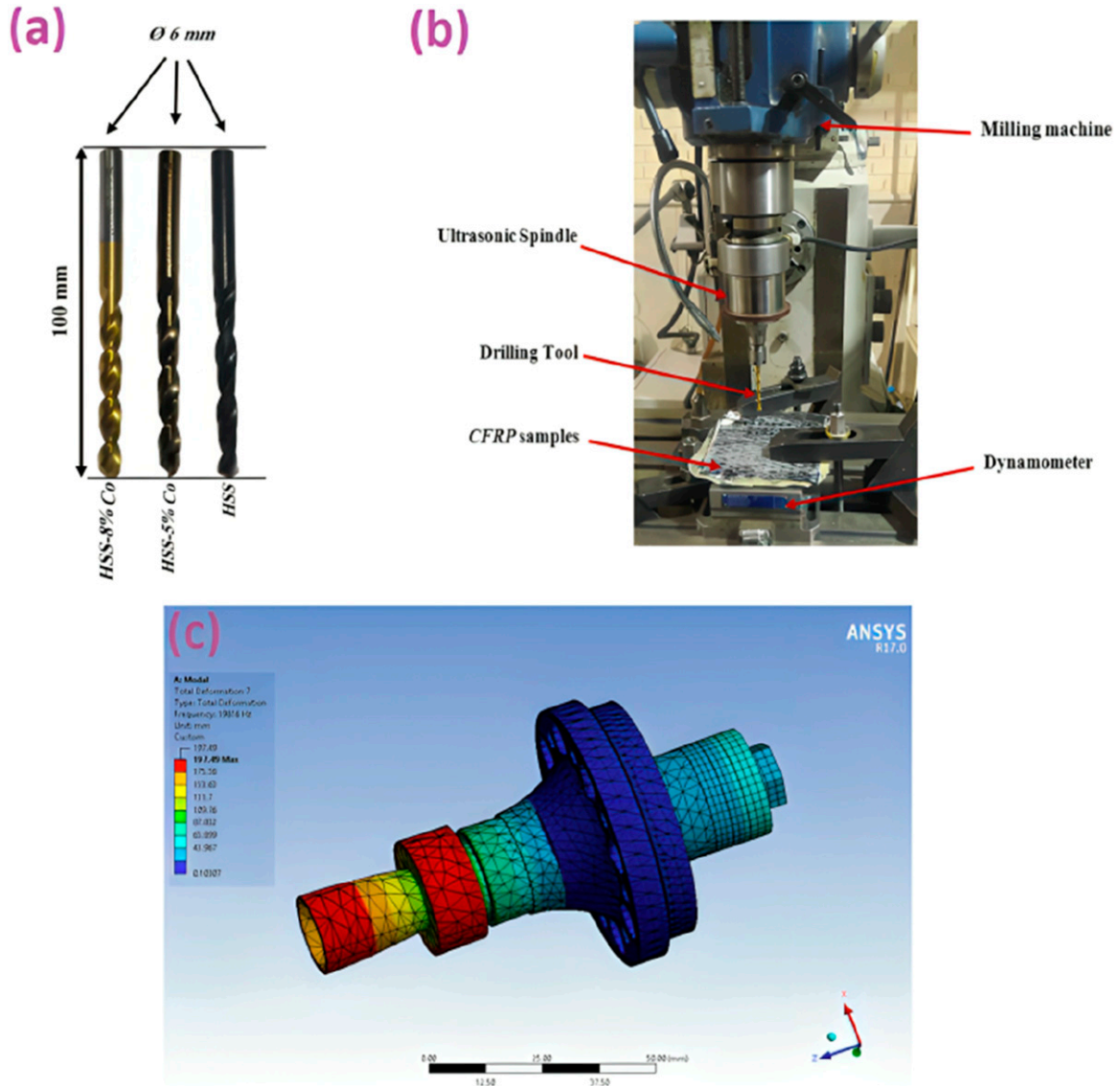


Figure 1. (a) The specifications of applied drilling tools, (b) the experimental test setup developed in-house for conducting the experiments, and (c) modal analysis of the horn structure to identify its vibrational modes and corresponding frequencies.

custom-designed experimental setup mounted on an FP4M CNC milling machine. Figure 1(b) illustrates the machine employed, operating within a spindle speed range of 50 to 2500 rpm, with a spindle motor power ranging from 3.7 to 4.4 kW for the main axis and 0.8 to 1.2 kW for the feed axis. It utilizes an A40 (M16)-DIN 2080 standard tool holder and supports a feed rate range of 8-630 mm/min. The machine X axis has a range of 500 mm, while the Y and Z axes each have a range of 400 mm. During the tests, axial forces were measured using a three-component Kistler piezoelectric dynamometer (Type 9257B), and the data were analyzed with Dynoware software.

To induce ultrasonic vibrations in the rotating tool, a specialized holder, connected to an AMMM type ultrasonic

vibration generator manufactured by MPI company, was utilized. To ensure efficient power transmission, an exponential geometry horn was employed to facilitate the transfer of ultrasonic energy from the holder to the drilling tool. The horn optimal geometry was determined through modal analysis conducted using ANSYS R17.0 software, revealing a resonance frequency of 19,816 Hz. Figure 1(c) presents the modal analysis results, illustrating longitudinal vibrations along the tool axis, with the highest deformation observed at the horn end, indicating effective vibration transmission to the tool. To facilitate vibration transfer, the horn material selection was critical, and Al-7075 was chosen for its suitable vibration transmission properties. The resonance frequency of the system was adjusted to 21 kHz,

and the amplitude of the tool vibration was monitored with a gap sensor, resulting in an approximate measurement of 6 μm .

Data acquisition and preprocessing

The experimental factors in this study were categorized into two groups: machining variables and materials variables. These factors, along with their respective levels, are presented in Table 3.

It is important to highlight the utilization of two drilling processes, namely non-ultrasonic (conventional) and ultrasonic-induced drilling, with the latter incorporating ultrasonic assistance. To efficiently explore the parameter space and minimize the number of experiments conducted, the Taguchi DoE technique was employed. This technique is renowned for designing high-quality systems and employs a specialized orthogonal array to comprehensively investigate the parameter space using a limited number of experiments. In this study, the experimental design was based on the L72 array, as per the Taguchi technique, and the specific array configuration is detailed in Table 4.

In this study, the conventional delamination factor $F_d = \frac{D_{max}}{D}$ was selected to analyze damage around the drilled hole based on several important considerations. Firstly, it offers a straightforward and easily interpretable measure of delamination by comparing the maximum delaminated area to the diameter of the hole, which is valuable for both academic research and practical industrial applications. Furthermore, this metric is commonly used in the literature,^{64,65} allowing for consistency and comparability with previous studies on drilling composites. The use of this factor ensures that our results are aligned with established research, facilitating meaningful comparisons. While more advanced delamination assessment methods could be considered in future research, this factor was deemed the most appropriate and effective for the objectives of this contribution.

This study utilized the Easson SP-4030 2D visual measurement machine (VMM), manufactured in China, for precise measurements and quantification of delamination. The VMM was specifically designed to provide magnification ranging from 0.7 \times to 4.5 \times . To measure the delamination, a series of points surrounding the damaged region were initially identified. Subsequently, the Rasson 2D software was utilized to generate a circle using the least square method, encompassing the selected points. Finally, by dividing the diameter of the resulting circle by the drill diameter, the delamination factor, referred to as F_d , was determined. This approach offers a systematic and reliable means of assessing the degree of delamination in the material under investigation. In addition, it is essential to highlight that this investigation includes an examination of peel-up delamination.

Table 3. Variation of process variables in the experimental study.

Input features	Level		
	1	2	3
Machining variables			
Ultrasonic vibration	OFF	ON	-
Tool type	HSS	HSS-5% Co	HSS-8% Co
Feed rate (mm/rev)	0.08	0.15	0.25
Material variables			
GNP wt.%	0	0.25	-
Arrangement	Asymmetric	Symmetric	-

In the present study, scanning electron microscopy (SEM) was employed to investigate the morphology of nanoparticles and carbon fibers embedded within the epoxy resin matrix. The utilization of SEM for particle size analysis was justified by its exceptional resolution capability, which extends up to 10 nm. This high resolution enables the detailed examination and characterization of the nanoscale features, thereby facilitating a comprehensive understanding of the composite system under investigation.

Machine learning methodology

Hyperparameter tuning and evaluation indicators

To construct, predict, and assess the performance of each individual base learner, the original database was divided randomly into two parts: a training set comprising 75% of the data and a testing set with 25% of the data. Ensuring the effectiveness of the model requires optimizing the hyperparameters involved. These external parameters are not part of the model and cannot be directly predicted from the dataset. However, they can be fine-tuned by efficient search techniques to achieve a satisfactory level of accuracy. The choice of the optimization approach depends on the number of key hyperparameters in the model and its complexity. Various tuning methods are employed to enhance the accuracy of learners by acting on the data and minimizing the expected generalization error over the hyperparameter search space. Predictions are evaluated against an independent test set or through techniques like cross-validation. Several search tactics are available, ranging from simple ones like random search or grid search to more advanced techniques like Bayesian optimization.⁶⁶

Grid search is a widely used method for hyperparameter tuning that involves exploring the performance of a model across all possible combinations of hyperparameter values. However, its main drawback lies in its computational cost, which increases with the number of hyperparameters and their levels, leading to longer processing times. To overcome these limitations and improve tuning performance,

Table 4. L72 array experimental design.

No.	Ultrasonic	Tool	Feed rate	GNP	Arrangement	No.	Ultrasonic	Tool	Feed rate	GNP	Arrangement
1	1	1	1	1	1	37	1	1	1	2	1
2	1	1	2	1	1	38	1	1	2	2	1
3	1	1	3	1	1	39	1	1	3	2	1
4	2	1	1	1	1	40	2	1	1	2	1
5	2	1	2	1	1	41	2	1	2	2	1
6	2	1	3	1	1	42	2	1	3	2	1
7	1	2	1	1	1	43	1	2	1	2	1
8	1	2	2	1	1	44	1	2	2	2	1
9	1	2	3	1	1	45	1	2	3	2	1
10	2	2	1	1	1	46	2	2	1	2	1
11	2	2	2	1	1	47	2	2	2	2	1
12	2	2	3	1	1	48	2	2	3	2	1
13	1	3	1	1	1	49	1	3	1	2	1
14	1	3	2	1	1	50	1	3	2	2	1
15	1	3	3	1	1	51	1	3	3	2	1
16	2	3	1	1	1	52	2	3	1	2	1
17	2	3	2	1	1	53	2	3	2	2	1
18	2	3	3	1	1	54	2	3	3	2	1
19	1	1	1	1	2	55	1	1	1	2	2
20	1	1	2	1	2	56	1	1	2	2	2
21	1	1	3	1	2	57	1	1	3	2	2
22	2	1	1	1	2	58	2	1	1	2	2
23	2	1	2	1	2	59	2	1	2	2	2
24	2	1	3	1	2	60	2	1	3	2	2
25	1	2	1	1	2	61	1	2	1	2	2
26	1	2	2	1	2	62	1	2	2	2	2
27	1	2	3	1	2	63	1	2	3	2	2
28	2	2	1	1	2	64	2	2	1	2	2
29	2	2	2	1	2	65	2	2	2	2	2
30	2	2	3	1	2	66	2	2	3	2	2
31	1	3	1	1	2	67	1	3	1	2	2
32	1	3	2	1	2	68	1	3	2	2	2
33	1	3	3	1	2	69	1	3	3	2	2
34	2	3	1	1	2	70	2	3	1	2	2
35	2	3	2	1	2	71	2	3	2	2	2
36	2	3	3	1	2	72	2	3	3	2	2

more advanced techniques, such as Bayesian optimization, can be employed. Unlike grid search, Bayesian optimization takes into account the influence of individual hyperparameters on the optimization process, resulting in more efficient tuning, especially for complex models.⁶⁷ Bayesian optimization is a powerful approach that consistently outperforms other global optimization techniques. It incorporates prior knowledge of an unknown function with observed data to derive a posterior distribution using Bayesian principles. By adopting this approach, the hyperparameter space can be effectively navigated, leading to more accurate results in a more efficient manner.⁶⁸

In the present study, hyperparameter tuning of single-parameter and more intricate multi-parameter models,

containing tree-based, boosting, and bagging algorithms was performed using grid search and Bayesian optimization techniques, respectively, coupled with cross-validation. It was considered that the hyperparameters' prior distribution followed a Gaussian distribution, enabling the efficient exploration of the hyperparameter space and informed decision-making to improve the model performance.

Predictive performance and effectiveness of base-learners and meta-model were quantitatively assessed by commonly used statistical metric indicators, including mean absolute error (MAE), root mean square error (RMSE), and coefficient of determination (R^2). The mathematical expression of each metric is provided as equations (1)–(3):

$$MAE = \frac{1}{N} \sum_{i=1}^N |y_i - \hat{y}_i| \tag{1}$$

$$RMSE = \sqrt{\frac{1}{N} \sum_{i=1}^N (y_i - \hat{y}_i)^2} \tag{2}$$

$$R = \frac{\sum_{i=1}^N (y_i - \bar{y}_i) (\hat{y}_i - \bar{\hat{y}}_i)}{\sqrt{\sum_{i=1}^N (y_i - \bar{y}_i)^2} \sqrt{\sum_{i=1}^N (\hat{y}_i - \bar{\hat{y}}_i)^2}} \tag{3}$$

where $y_i, \hat{y}_i, \bar{y}_i,$ and $\bar{\hat{y}}_i$ represent the real, predicted, average real, and average predicted response values, respectively, and N denotes the total number of sample points.

The specifications of proposed stacked generalization method

Base-learner adaptation. Figure 2 depicts the process of transforming base learners into adapted input instances for the meta-model. Initially, the dataset was partitioned into four separate folds, with three of them dedicated to training, and the remaining fold used as the validation set. The training process for each learner was iterated four times, corresponding to the number of folds, to build the adapted

training and validation sets for the stacked model. This approach allows the meta-model to acquire more information from the base learners, resulting in more robust and accurate predictions. Each iteration also involved ten-fold cross-validation to enhance the model robustness. Following the transformation of the training and sets into adapted instances, they were employed for training and prediction of the meta-learner, respectively, as illustrated in Figure 3. The converted test sets and its performance were evaluated using specific metric indicators.

Selection of base learners. To boost the efficacy of the stacked model, the prediction accuracy of different single ML models was assessed and four best-fit models were selected to serve as the input first-level learners for the ensemble stacking approach used in this study, as illustrated in Figure 4. The model performance was evaluated via RMSE values of the corresponding model, as a robust indicator of predictive accuracy in ML. Lower RMSE values indicate better fitness to the training data. Model selection involved two main classifications: non-ensemble and ensemble tree-based algorithms. Considering the potential for improved performance through ensemble models, which harness the collective impact of multiple learners, one and three candidates were selected from the non-ensemble and ensemble groups, respectively. This approach aims to combine the strengths of both single learners and ensemble

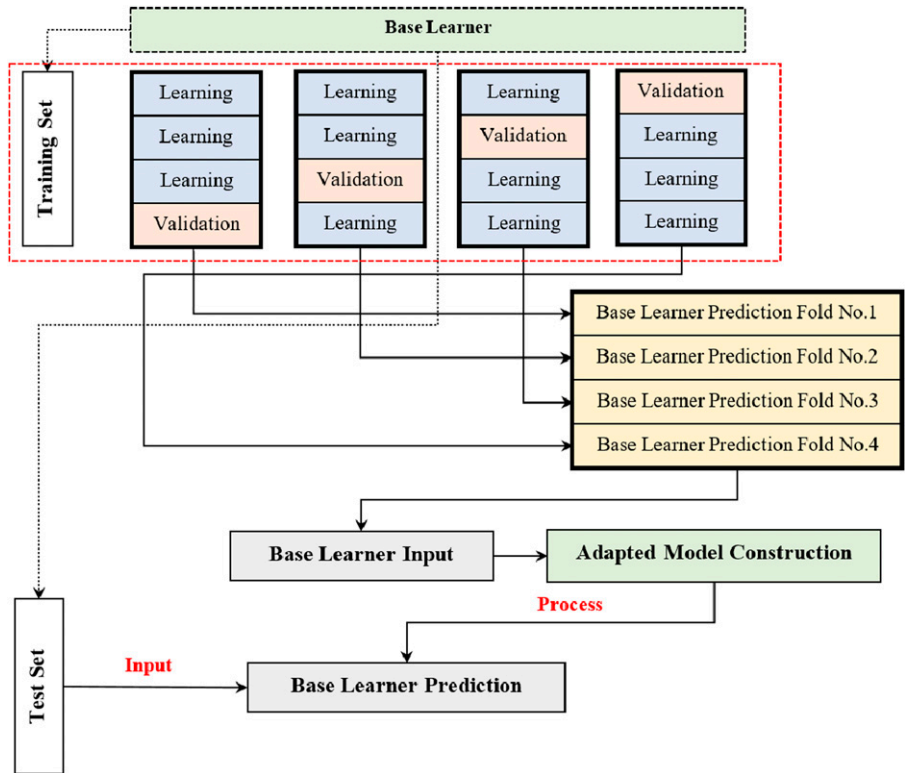


Figure 2. Adaptation of base learners as the precursor for constructing the stacked ensemble meta-model.

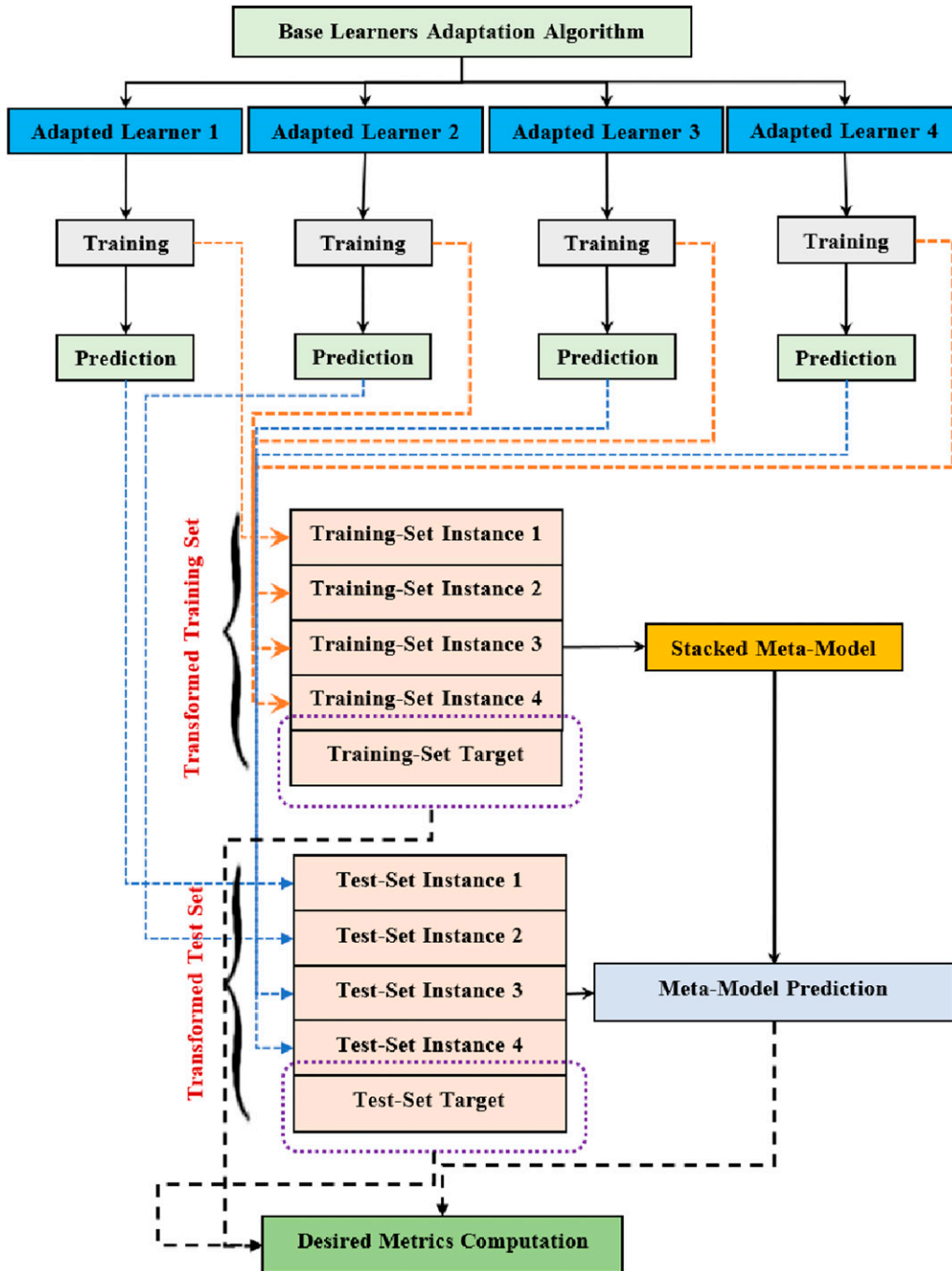


Figure 3. A schematic illustration of implementing transformed base learners according to stacked generalization.

methods to enhance the overall predictive capability of the final stacked model.

Model optimization. In this study, SGBR was employed to construct the meta-learner, and Bayesian optimization was applied to optimize its hyperparameters. Figure 5 illustrates the overall process for Bayesian optimization of the meta-

learner hyperparameters for best-tuning. The optimization problem was formulated to minimize the RMSE between the meta-model predictions and the actual test set outputs. The specific hyperparameters required for SGBR, along with their corresponding operation ranges, are presented in Table 5. The adoption of Bayesian optimization was crucial due to the considerable number of hyperparameters with

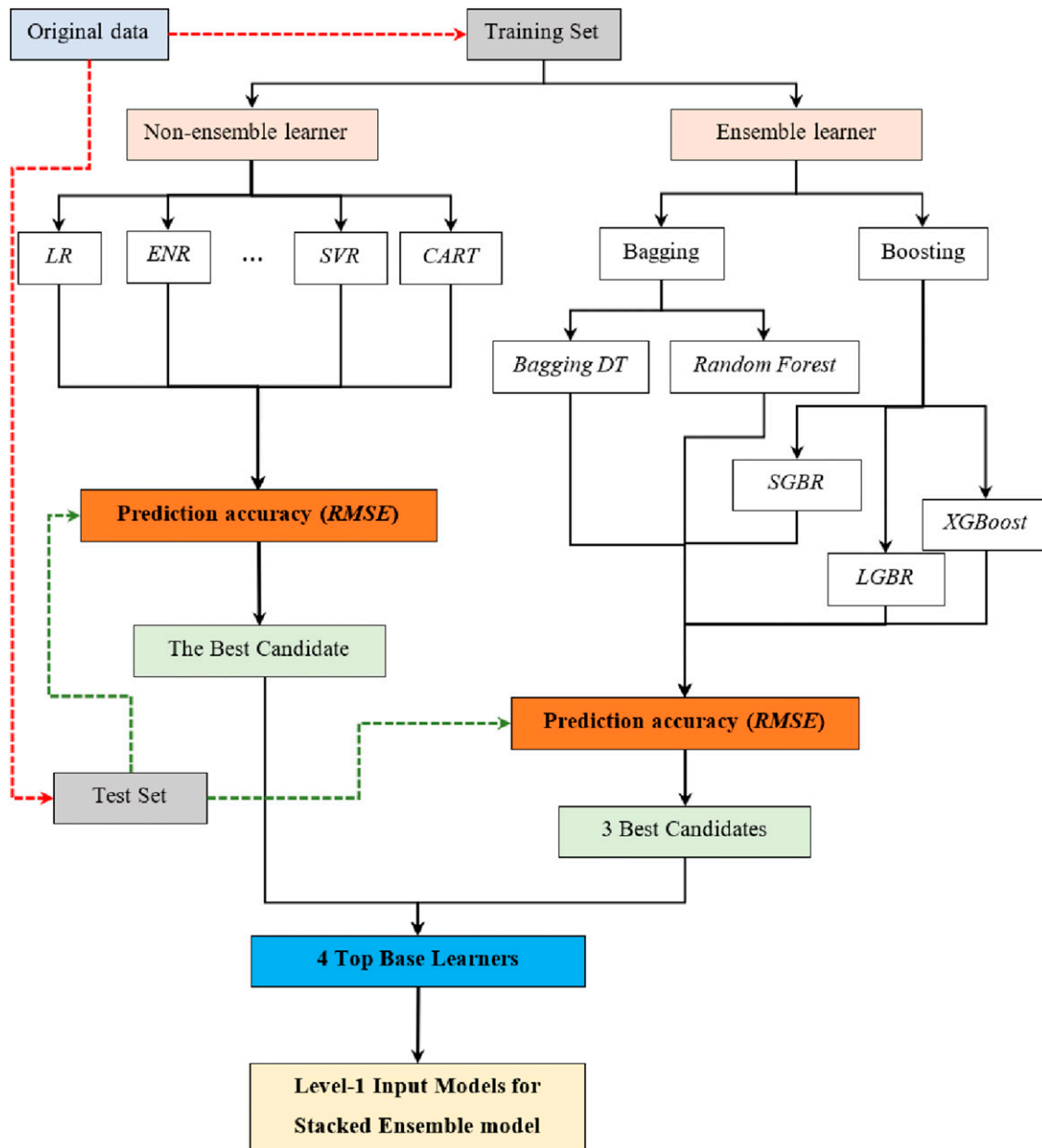


Figure 4. The selection procedure for most appropriate input models as first-level base learners of the stacked metamodel.

wide working ranges, significantly enhancing the robustness and prediction accuracy of the stacked SGBR model.

Nested feature scoring (NFS)

Feature importance analysis is one of the versatile secondary products of ML models, by which the effects of each instance variation on the overall characteristics of the output can be scored. The metric for feature scoring may vary for different learners, as each model uses a distinct measuring system for importance analysis. For instance, the average Gain of an instance during node

splitting is computed by XGBoost.⁶⁹ On the other hand, in RF, the Gini impurity or mean squared error impurity criterion is used to rank the importance of the corresponding feature. Lower impurity values are associated with greater levels of importance for the variable.⁷⁰ For categorical variables with different levels, the sub-feature analysis also plays a key role in significance analysis. It is hence beneficial to consider the effects of these sub-instance features during feature scoring. NFS was hence developed in the present study for the feature scoring and determining each sub-feature contribution within the corresponding independent instance.

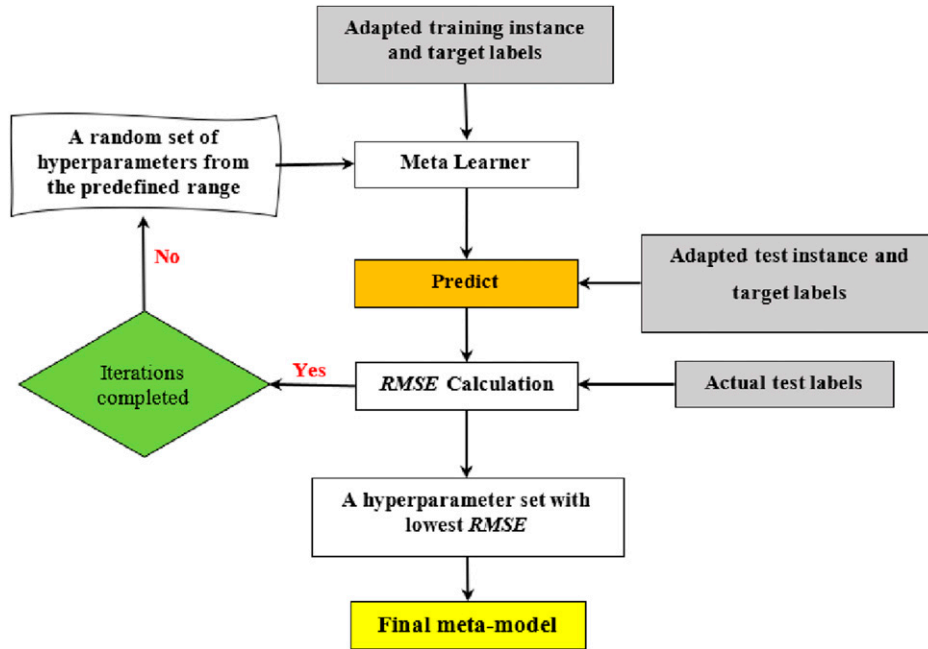


Figure 5. Bayesian process for optimization of meta-learners' tuning hyperparameters.

Table 5. The specifications and operation range of hyperparameters for the adopted SGBR meta-learner.

Hyperparameter	Technical terminology	Range
n.trees	Boosting Iterations: The count of trees in gradient boosting	100–1000
interaction.depth	Maximum number of nodes in each tree	1–10
Shrinkage	Learning rate	0.1–1
n.minobsinnode	Minimum number of observations in terminal nodes of each individual tree	5–10
bag.fraction	Fraction of the training set observations randomly selected to create the next tree in the expansion	0.5–0.8

The flowchart for nested importance analysis is shown in Figure 6. The process began with building SGBR, RF, and XGBoost models using both discrete factors (ultrasonic, tooling type, material, and lay-up) and a continuous variable (feed rate). Each feature scoring algorithms determined the significance ratios of these features. These ratios were then normalized to a scale of 0 to 1, with the lowest and highest significance effects mapped to 0 and 1, respectively. For sub-feature scoring, one-hot encoding was used to convert categorical variables into binary forms, making them easier for machine learning algorithms to handle and improving the model fitting efficiency, particularly for nonlinear variations. This approach provided a clearer understanding of feature importance. The one-hot encoded data was used to build the models, and scores were normalized again for comparison. Finally, the normalized scores for nominal features were adjusted based on their main features' scores to determine the relative importance of each sub-variable. The importance

results were then compiled from the normalized features and sub-features. The evaluation used SGBR, XGBoost, and RF models, each with its own ranking system. The average scores from these models were calculated to ensure accuracy, with the feed rate considered separately as a regression variable.

Results and discussion

Microstructural characteristics of the hybrid composite laminates

Fiber-matrix interaction analysis. To examine the micro- and nano-structures of both CFRP and CFRP/GNP samples before the drilling process, specific sections of the samples were intentionally fractured at cryogenic temperatures, ensuring a brittle fracture behavior. The resulting images are displayed in Figures 7 and 8. In Figure 7(a), a closer view (125x) of CFRP laminates reveals the bonding between

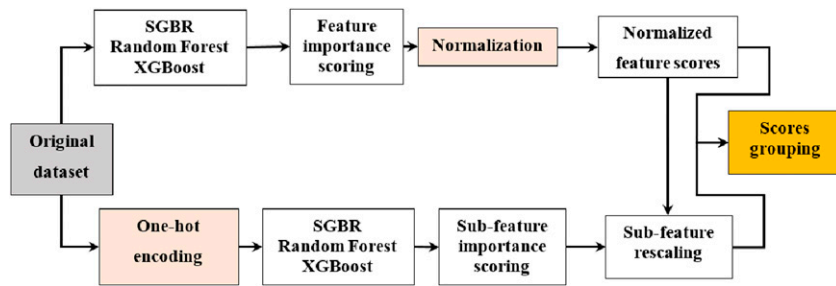


Figure 6. Nested feature importance analysis based on sub-feature rescaling.

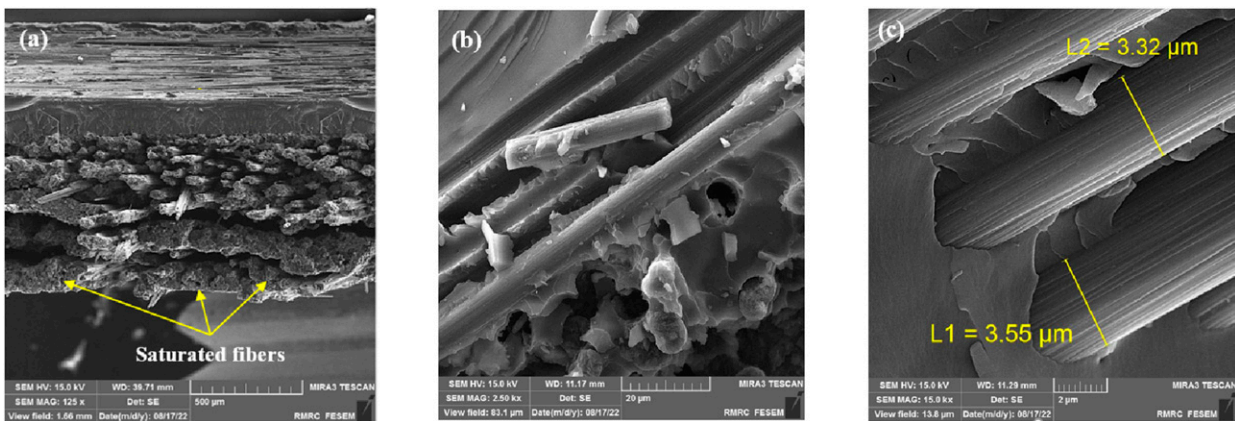


Figure 7. SEM images of CFRP laminates: (a) low magnification showing effective fiber saturation by epoxy resin, (b) higher magnification highlighting successful fiber pre-impregnation, and (c) uniformly aligned fibers with high resin saturation.

carbon fibers and epoxy resin, demonstrating effective fiber saturation. **Figure 7(b)** offers an enlarged perspective of carbon fibers within the epoxy, confirming successful pre-impregnation. This confirms the epoxy successful attachment to the carbon fibers. Furthermore, **Figure 7(c)** highlights the presence of unidirectional carbon fibers, each approximately 3.3 mm in diameter. These fibers were completely aligned in a single direction and were saturated using the hand layup method.

Nanoparticle distribution in hybrid laminates. **Figure 8** presents the integration of GNPs into CFRP composites. In **Figure 8(a)**, epoxy resin is shown, containing GNPs. **Figure 8(b)** provides a high-magnification SEM image extracted from **Figure 8(a)**, revealing a single GNP approximately 500 nm in size. The distribution of GNPs within the carbon fiber/epoxy matrix is shown in **Figure 8(c)**, demonstrating a favorable dispersion that contributes to beneficial mechanical effects. However, some localized agglomeration of GNPs is evident in certain areas, as shown in **Figure 8(d)**. This agglomeration could potentially reduce ductility. Such agglomerates might weaken the interfacial load transfer between the epoxy and GNPs,⁷¹

increasing the material vulnerability to fracture under mechanical stresses like drilling forces.

Feature importance analysis

The impact of input variables on the delamination and thrust force during the drilling process can be assessed through feature importance analysis as detailed in the following subsections.

Delamination. **Figure 8** present the NFS-based importance assessment results for SGBR, RF, XGBoost, and their average values, along with the normalized sub-feature scoring results (prior to rescaling) for delamination. The scoring algorithm involved normalizing the main features, projecting their minimum and maximum scores to 0 and 1, respectively. Sub-instances were subsequently rescaled based on the features' normalized scores after their first-stage normalization, allowing for the identification of the portion they occupy within their group. The importance values of both main and sub-features on delamination, with a focus on model-averaging for both normalized and

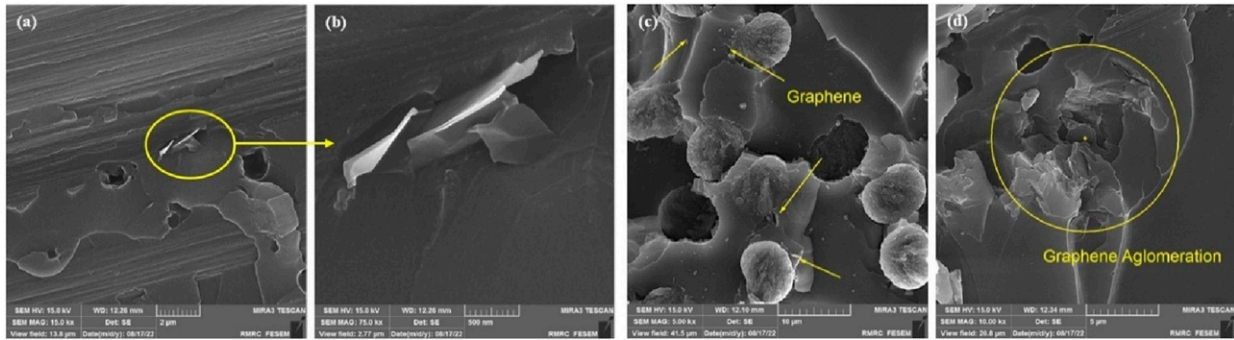


Figure 8. SEM images of CFRP composites with GNPs: (a) low magnification of epoxy matrix with a GNP, (b) higher magnification of the GNP nanoplate, (c) example of uniform GNP dispersion, and (d) evidence of GNP nanosheet agglomeration.

Table 6. The averaged NFS results.

Output	Main feature	Normalized FS	Sub-feature	Normalized FS	Rescaled FS			
Delamination	Material	0.2560	CFRP	0.4371	0.2102			
			Nano-reinforced CFRP	0.1022	0.0458			
	Lay-up	0.0921	Symmetric	0.0629	0.0329			
			Asymmetric	0.4491	0.0592			
	Ultrasonic	0.0087	ON	0.0051	0			
			OFF	0.4146	0.0087			
	Tooling type	I	0.4692	HSS	0.6776	0.4716		
				HSS-5% Co	0.6154	0.4267		
				HSS-8% Co	0.1411	0.1016		
				Feed rate	0.1364	CFRP	Feed rate	I
Nano-reinforced CFRP							0.0918	0.1342
Symmetric							0.0102	0.0022
Lay-up	0.0793	0.0420	Asymmetric	0.1256	0.0283			
			Ultrasonic	0.0402	ON	0.0034	0.0006	
Tooling type	0.4907	0.1108	OFF	0.1108	0.0396			
			HSS	0.1003	0.1940			
			HSS-5% Co	0.1276	0.2372			
			HSS-8% Co	0.0382	0.0594			
			Feed rate	I	0.0382	Feed rate	I	I

rescaled states, are also listed in Table 6 to provide more clarification.

Drilling-induced delamination typically manifests at both the entry and exit regions of a drilled hole, resulting in the formation of a delamination zone characterized by its maximum diameter. The feature importance analysis for delamination implies that higher scores for an input category are associated with more determining effects on the quality of the part. Similarly, the sub-feature score analysis indicates that higher importance scores for a sub-variable correspond to a more significant effect compared to sub-features with lower scores. In Figure 9a–(d), it can be observed that the most significant factor affecting delamination is the tool type, followed by the feed rate. The third significant variable alternates between layup and material; however, the average results suggest that the material type is

the third most important feature. On the other hand, ultrasonic implementation exhibits the least importance on delamination compared to machining and material parameters, highlighting the dominant effects of machining parameters in altering delamination.

In Figure 9(e), the results of sub-feature scoring, conducted without feature-based rescaling, reveal the significant role played by the feed rate in comparison to other sub-components of the input data. Notably, the feed rate, considered as a continuous variable, exhibits cumulative importance across its three sub-levels (0.08, 0.15, and 0.25 mm/rev). Additionally, the selection of the tool, specifically HSS and HSS-5% Co, exerts a substantial effect on delamination, while increasing the cobalt content to 8% did not lead to further impact on the final delamination. By comparing the score ratio of non-reinforced CFRP to the

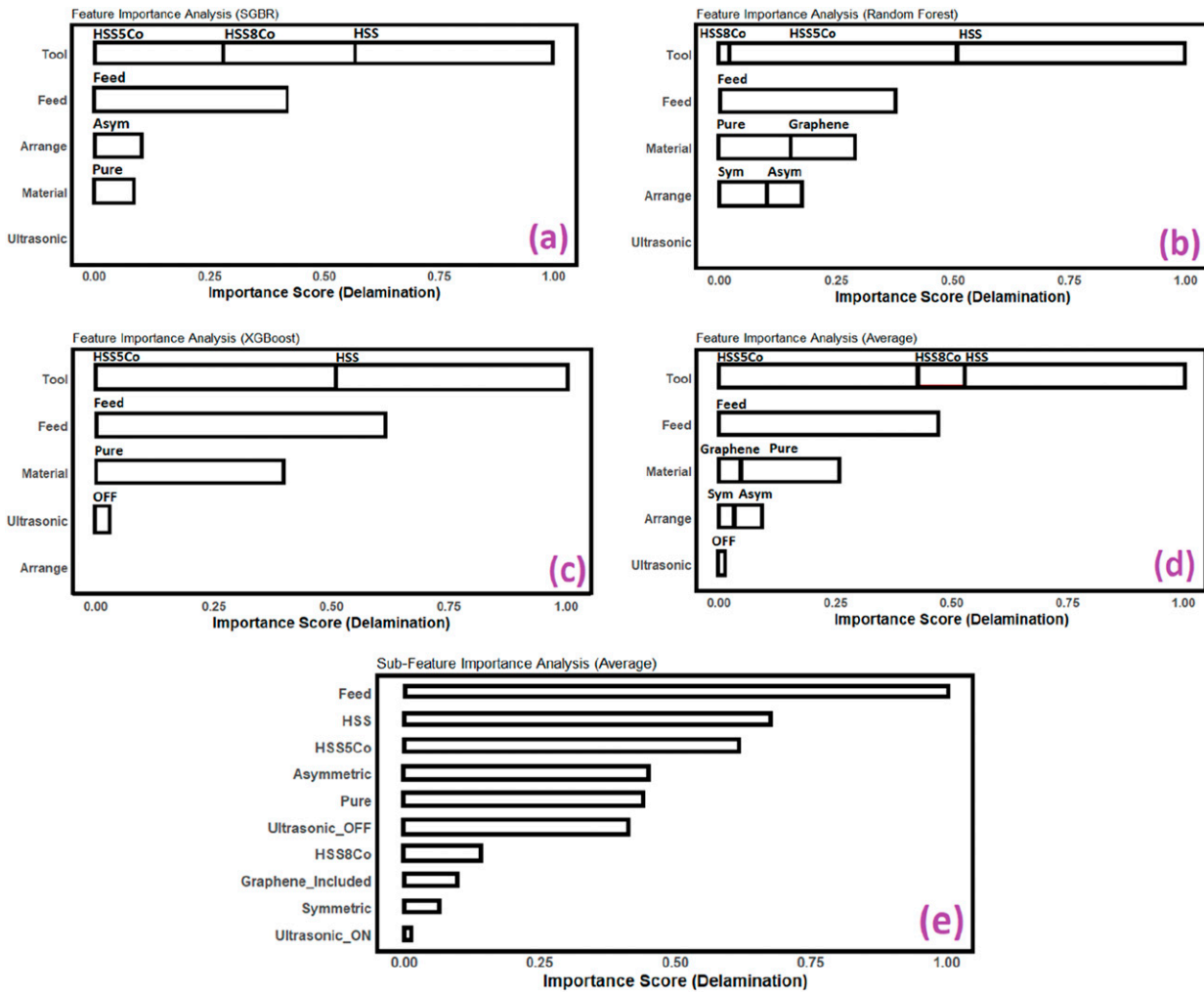


Figure 9. The NFS analysis for delamination based on (a) SGBR, (b) RF, (c) XGBoost, and (d) model averages, and (e) normalized sub-feature scoring.

reinforced state in Figure 9(d) and (e), it is evident that the inclusion of GNP caused minor effects in delamination behavior. The comparative analysis of layup sub-features in Figure 9(d) and (e) demonstrates the dominance of asymmetric layup over symmetric structures in affecting delamination. Furthermore, it is evident from these Fig. s that altering the drilling state from conventional state to ultrasonic drilling did not shift the delamination value to a significant extent.

Thrust force. Based on the findings from Figure 10, it is evident that the feed rate emerged as the most influential feature on the failure force, showing a marked rise in importance against the previous state. As the second most significant factor, except for the RF model, the remaining models favored the tool type. Additionally, the machining factors demonstrated notable importance in altering the thrust force compared to other options. As depicted in

Figure 10, the material options ranked third in importance, with the non-reinforced option having a larger share than the hybrid CFRP. The layup structure came in fourth, with the asymmetric structure being more prevalent. Similar to delamination, the incorporation of ultrasonics was not as effective as other factors, as shown in Figure 10(d), although it displayed a higher score on affecting the thrust force. Upon independent analysis of sub-features in Figure 10(e), it was apparent that the feed rate showed much greater importance compared to other sub-features, while other parameters presented lower significance. Notably, the tooling type was more impactful on failure force when using HSS and HSS-5% Co, and the asymmetric structure dominated over the symmetric one. Similarly, the addition of GNP and implementing ultrasonic vibrations did not lead to significant variations in thrust force, with respect to other input variables, during the drilling process.

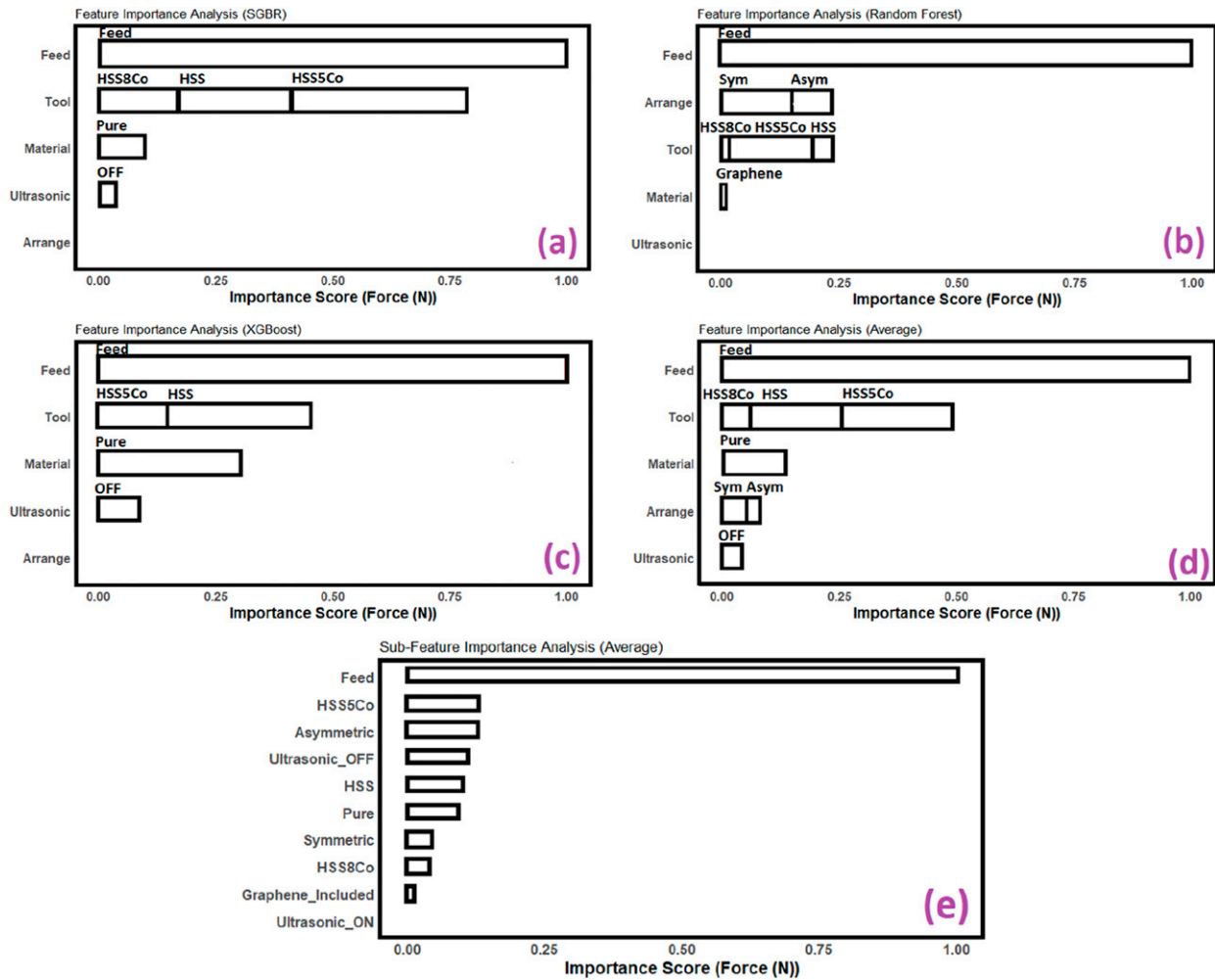


Figure 10. The NFS analysis for thrust force based on (a) SGBR, (b) RF, (c) XGBoost, and (d) model averages, and (e) normalized sub-feature scoring.

The proposed stacked ensemble implementation

As previously mentioned, the stacked generalization technique necessitates the selection of several best-fit algorithms before the stacked ensembling process can be conducted. Consequently, various non-ensemble and ensemble ML algorithms were tested, and their prediction efficiency, based on predefined performance metrics, was comparatively assessed to identify the four most suitable models. Initially, several non-ensemble ML models were trained by randomly selecting 75% of the sample points obtained from experiments, and the remaining points were used for testing. To improve the prediction efficiency, Bayesian optimization and grid search techniques were employed to optimize the models with multiple and limited hyperparameters, respectively.

Non-ensemble base learner assessment. Table 7 displays the performance measures concerning the assessment of single non-ensemble learners. The evaluation primarily focused on

the most commonly used practical models. From Table 7, it can be observed that generalized linear regression models, such as Ridge regression, Elastic Net, and Bayesian regression, exhibited low levels of accuracy and R-squared index, indicating limited generalizability for predicting test sample points. This trend was also observed for more complex models like support vector regression (SVR) and k-nearest neighbor regression (kNN). In contrast, improved performance metrics, characterized by lower error and higher R-squared index for both responses, were demonstrated by the classification and regression tree (CART) model. This superiority can be attributed to the model's higher efficiency in handling data containing categorical input variables, increased flexibility in capturing complex non-linear intervariable and input-response interactions, and reduced sensitivity to outliers, with respect to other non-ensemble learners. Due to comparatively pronounced accuracy, the CART approach was adopted as the non-ensemble base learner for the stacked model.

Table 7. The performance of non-ensemble single models to predict delamination and thrust force.

Method	Delamination			Thrust force		
	MAE	RMSE	R ²	MAE	RMSE	R ²
Linear Regression	0.0158	0.0183	0.5548	28.50	34.00	0.5130
Ridge Regression	0.0177	0.0220	0.2892	27.29	33.78	0.5323
Elastic Net Regression	0.0194	0.0248	0.0288	27.80	34.42	0.5143
Bayesian Regression	0.0157	0.0183	0.5576	28.47	33.97	0.5133
Kernel Ridge Regression	0.0174	0.0207	0.3727	24.80	32.18	0.6746
Robust Regression	0.0157	0.0185	0.5632	29.76	35.69	0.4766
Support Vector Regression	0.0166	0.0204	0.5447	23.96	30.52	0.6200
K-nearest Neighbor Regression	0.0168	0.0198	0.4661	36.80	42.39	0.1963
CART	0.0127	0.0161	0.6907	21.81	26.62	0.6921

Ensemble tree-based single learner assessment. Several popular methods with boosting and bagging capabilities, such as Bagging Decision Tree (BDT), SGBR, RF, Light Gradient Boosting Regression (LGBR), and XGBoost, were chosen to evaluate their potential as ensemble base learners with their demonstrated effectiveness in Table 8. The performance was assessed using MAE, RMSE, and R-squared index estimators, and the results were tabulated in Table 8. The values of MAE and RMSE when utilizing ensemble techniques were generally found to be lower than those of non-ensemble models (with the exception of CART). This trend indicates that the inclusion of ensembling improved the fitting accuracy compared to models without ensembling, as shown in Table 8. Among the models, SGBR, LGBR, and XGBoost demonstrated the lowest errors and highest R-squared measures. Based on this finding, the three approaches with boosting capability were selected as ensemble-based input learners for the stacked model.

The stacked model construction and performance evaluation. Based on the assessments detailed in previous sections, the CART, SGBR, LGBR, and XGBoost algorithms emerged as the most effective for predicting delamination and output in composite drilling processes. The CART model uses a tree-based approach to create simple, interpretable rules for categorical or regression targets, employing binary splits at each level until a maximum depth is reached.⁷² SGBR builds a robust model by iteratively training on random subsets of data with gradient descent to minimize loss, effectively handling imprecise and imbalanced datasets while managing non-linear relationships and outliers.⁷³ XGBoost enhances gradient boosting by introducing regularization to prevent overfitting.⁷⁴ LGBR, an advanced variant of XGBoost, improves training speed and efficiency by using vertically grown trees, offering superior performance compared to earlier models.⁷⁵

In the stacking technique, the SGBR method was used to create the meta-model, with hyperparameters fine-tuned

Table 8. Performance measures of boosting- and bagging-based ensemble methods.

Method	Delamination			Thrust force		
	MAE	RMSE	R ²	MAE	RMSE	R ²
BDT	0.0152	0.0178	0.6174	25.24	29.91	0.5866
SGBR	0.0135	0.0154	0.6975	20.12	25.14	0.7560
LGBR	0.0096	0.0130	0.7633	14.82	21.47	0.8273
RF	0.0140	0.0168	0.6381	25.33	29.41	0.6192
XGBoost	0.0130	0.0157	0.6381	22.61	27.71	0.6446

through Bayesian optimization. Table 9 shows the results of the optimized stacked ensemble model for predicting delamination and thrust force. Metric estimators were employed to compare the performance of base learners, including the Ridge regression model, with the stacked meta-learner. The base tree-based ensemble learners outperformed non-ensemble models, showing better fitting and generalization. The Bayesian-optimized two-stage stacking ensemble further improved performance, surpassing individual base learners in predicting both delamination and thrust force for training and test sets. The stacked meta-model achieved an R-squared value of 1 with MAE and RMSE scores of 0 for both responses in the training set, indicating exceptional performance with limited data and numerous input variables. This approach significantly reduced MAE and RMSE—by about 97% and 124% for delamination, and 205% and 154% for thrust force—compared to the LGBR algorithm, the best-performing base learner. These results highlight the effectiveness and superiority of the stacked ensemble method in this context.

The predictive performance of the meta-model is shown in Figure 11 for both training and test sets, as well as the entire dataset. The Fig. includes solid and dashed lines representing the $y = x$ line and the linear regression line

Table 9. The comparison of different base learners performance with that of the proposed stacked ensemble algorithm.

Factor	Set	Algorithm					
		Ridge	CART	SGBR	LGBR	XGBoost	Ensemble
Train set							
Delamination	R^2	0.1869	0.5426	0.6909	0.8268	0.5322	1
	MAE	0.0145	0.0106	0.0095	0.0059	0.0109	0
	RMSE	0.0178	0.0133	0.0111	0.0082	0.0135	0
Thrust force	R^2	0.3772	0.4356	0.6106	0.7446	0.6189	1
	MAE	33.28	29.81	24.52	18.98	23.53	0
	RMSE	40.68	38.72	32.64	26.48	31.90	0
Test set							
Delamination	R^2	0.2892	0.6907	0.6975	0.7633	0.6381	0.9661
	MAE	0.0177	0.0127	0.0135	0.0096	0.0130	0.0038
	RMSE	0.0220	0.0161	0.0154	0.0130	0.0157	0.0058
Thrust force	R^2	0.5323	0.6921	0.7560	0.8273	0.6446	0.9732
	MAE	27.29	21.81	20.12	14.82	22.61	4.8538
	RMSE	33.78	26.62	25.14	21.47	27.71	8.4416

for the data points. The close alignment of these lines indicates how well the model predictions match the actual values. Figure 11(a) demonstrates that the regression lines closely follow the $y = x$ line, reflecting accurate predictions and efficient training. Figure 11(b) highlights the model accuracy in predicting responses, with the accuracy line closely aligning with the actual values. Finally, Figure 11(c) confirms the meta-model ability to effectively predict delamination and thrust force across the entire dataset, showcasing the model overall accuracy.

Visual and statistical assessment

To investigate deeper into the impact of independent factors on delamination and failure thrust force, a series of statistical analyses were carried out based on main effects analysis. This method can determine the average response for each specific input level and reveal the relative influence of each input parameter in comparison to the others. The detailed findings and corresponding explanations are provided in the following sub-sections.

Delamination. Figure 12 displays the main effects plots illustrating the connection between delamination and different inputs. To complement the main effects analysis for delamination assessment, visual representations of post-drilled holes with their corresponding delamination factors were included in Figures 13–17 under various settings. In Figure 12(a), the variation in delamination between ultrasonic-assisted and conventional drilling was found to be relatively minor, which aligns with the feature scoring analysis discussed in section 4.2.1. However, previous

research, such as ⁷⁶, showed that ultrasonic vibrations can have a more substantial impact on reducing delamination. In this study, while ultrasonic assistance led to a reduction in thrust force, the effect on delamination was less significant than anticipated. This outcome may be influenced by several experimental factors, including the specific amplitude of ultrasonic vibrations, the geometry of the tool, and the material unique response to the combined effects of ultrasonic vibration and drilling parameters. It is possible that the ultrasonic vibration frequency or amplitude used in this work did not reach the optimal range for achieving a notable reduction in delamination. Moreover, the presence of GNPs and other material properties may have interacted with the ultrasonic vibrations in ways that altered the delamination behavior. Future studies could examine a wider range of ultrasonic parameters and compare them with the conditions used here to gain deeper insight into the mechanisms affecting delamination reduction. Figure 13 illustrates and quantifies the comparison between delamination under non-ultrasonic and ultrasonic-assisted drilling. The delamination factor magnitudes depicted in Figure 13 show that conducting ultrasonic-induced experiments resulted in a slight decrease in delamination factor in comparison to the non-ultrasonic tests. This improvement can be attributed to the intermittent nature of the ultrasonic drilling process, which facilitates the cutting of fibers and consequently reduces the occurrence of machining-induced damage.⁷⁷ As evident in Figure 13(a), it's noticeable that the damaged area along the hole boundaries was more pronounced under non-ultrasonic conditions compared to when ultrasonic assistance was employed.

In Figure 12(b), the impact of different tooling types on delamination variation is illustrated. Based on Figure 12(b),

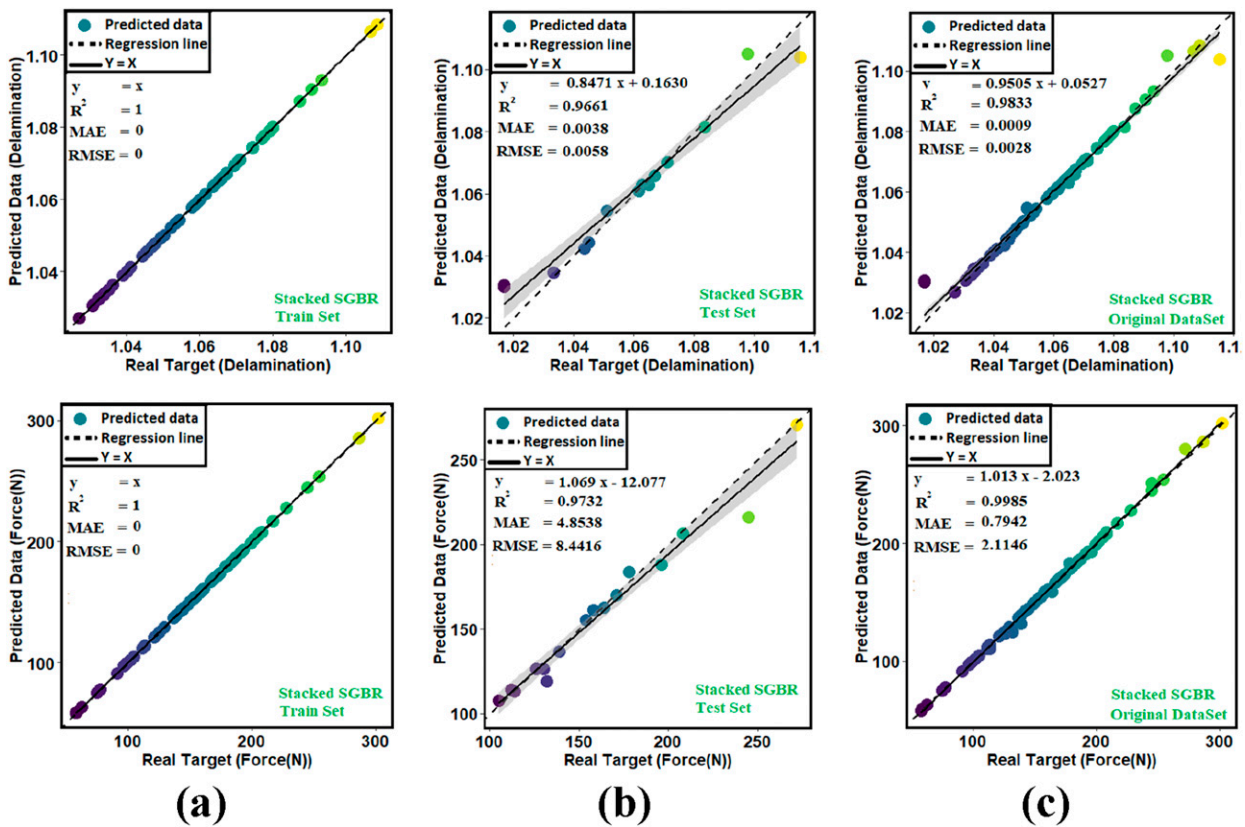


Figure 11. Graphical illustration of the proposed stacked generalization strategy for predicting (a) training, (b) testing, and (c) the entire dataset.

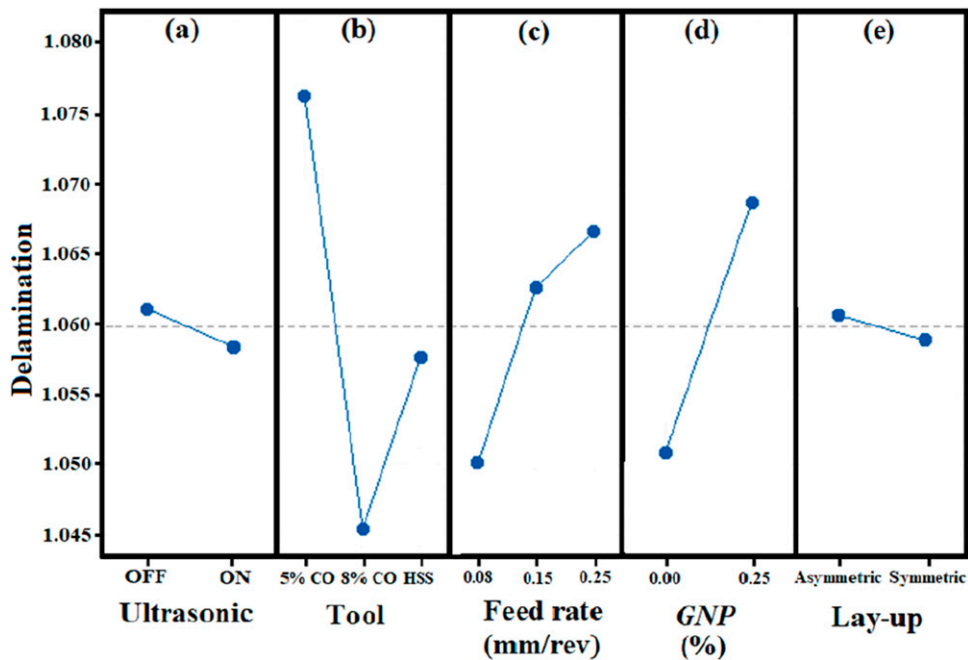


Figure 12. Main effects plots showing delamination variation with respect to (a) ultrasonic activation, (b) tool type, (c) feed rate, (d) GNP content, and (e) lay-up configuration.

the average delamination factor exhibited the highest variations across the diverse tool types, aligning with the tool's elevated importance score for delamination, as discussed in section 4.2.1. HSS tools are commonly utilized in the industry due to their cost-effectiveness and strength. However, the incorporation of cobalt into HSS tools enhances their durability and wear resistance. This enhancement is evident in Figure 14(b), where holes drilled using the HSS-8% Co tool displayed reduced delamination ($F_d = 1.0402$). The increase in cobalt content up to 8% in the HSS tool proved to be beneficial for drilling CFRP. In contrast, the HSS-5% Co tool resulted in the most significant delamination damage ($F_d = 1.0791$) among all applied tools. Consequently, the HSS-8% Co type emerged as the most effective among the HSS family tools for minimizing delamination. As a clear validation, the drilled hole quality is visibly improved when using HSS-8% Co as the cutting tool, as depicted in Figure 14(c). In contrast, Figure 14(a) and (b) exhibit evident surface damage with noticeably higher levels of roughness. Babu et al.⁷⁸ investigated the performance of different cutting tools—HSS, HSS Co, and solid carbide—during the drilling of pure CFRP. Their results showed that the HSS Co (M42) tool exhibited superior performance compared to the HSS (M35) tool, demonstrating better overall drilling efficiency.

Figure 15 visually demonstrates the impact of different feed rates on delamination. Based on NFS analysis in Figure 9, feed rate played a substantial role in delamination during drilling, as also affirmed in Figure 12(c) where the notable variation of delamination with feed rate was evident. Yaşar et al.⁷⁹ emphasized that feed rate plays a crucial role in influencing delamination during the drilling of CFRP composites. Similarly, Shyha et al.,⁸⁰ supported this observation, showing that both the type of drill bit and the feed rate are significant factors affecting thrust force and delamination. These findings collectively highlight the critical impact of feed rate and tool selection on drilling performance in CFRP, reinforcing the need for careful parameter optimization in minimizing delamination. The trends in delamination levels within Figure 15 indicate a clear correlation: higher feed rates led to increased drilling-induced delamination, while lower feed rates correlated with reduced delamination. This is due to the easier cutting of carbon fibers at lower feed rates, resulting in decreased delamination. Conversely, higher feed rates can pull fibers instead of cutting them, leading to increased delamination. Additionally, higher feed rates generally lead to increased thrust force, contributing to greater material damage around the hole. The visual depictions in Figure 15 also illustrate that a feed rate of 0.08 mm/rev resulted in smoother hole

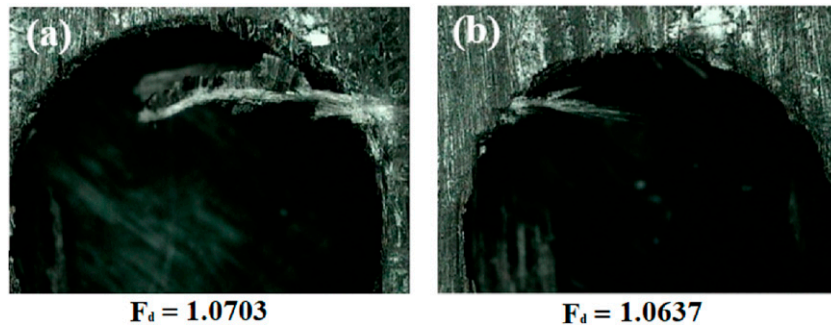


Figure 13. The drilled holes subjected to two different processing techniques: (a) non-ultrasonic process and (b) ultrasonic-induced process.

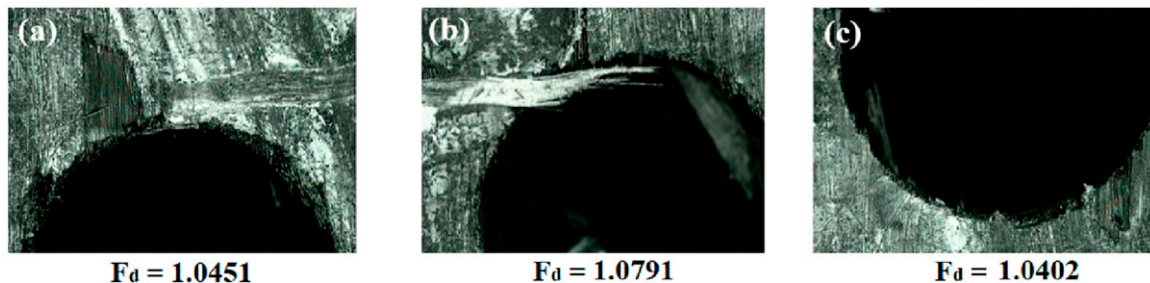


Figure 14. Visualization of the drilled holes by (a) HSS, (b) HSS-5% Co, and (c) HSS-8% Co drilling tools.

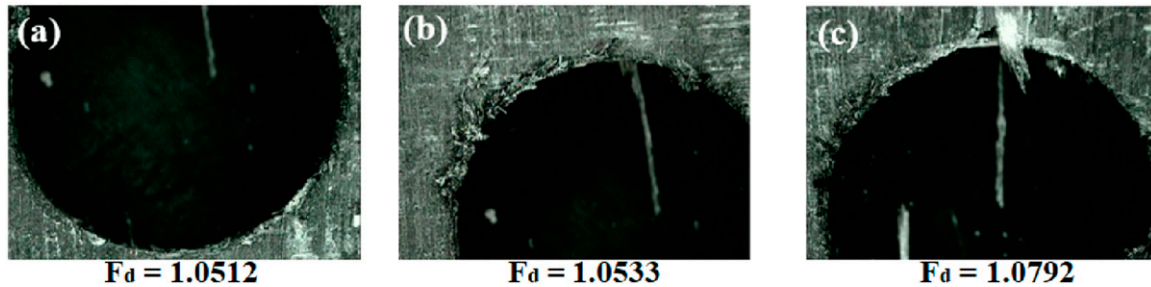


Figure 15. Illustration of the drilled holes at feed rates of (a) 0.08, (b) 0.15, and (c) 0.25 mm/rev.

boundaries and limited damaged region compared to a feed rate of 0.15 mm/rev.

In [Figure 12\(d\)](#), a notable impact on material delamination was evident based on the material type, as also reinforced by the feature scoring in section 4.2.1. This observation was consistent with both [Figures 12\(d\)](#) and [16](#), indicating that the inclusion of GNP led to increased delamination factor. This effect can be attributed to the enhanced strength of the CFRP material with GNP incorporation. The higher material strength contributed to greater cutting forces during failure, subjecting the fibers to increased tension forces during drilling. Consequently, this resulted in more significant degradation of the hole periphery, as demonstrated in [Figure 16](#). Visual representations of the drilled holes in [Figure 16](#) further support this finding. The smoother surface and limited surface failure extent around the hole for CFRP in [Figure 16\(a\)](#), in contrast to [Figure 16\(b\)](#) where GNP was incorporated, highlight the influence of GNP on delamination behavior during the drilling process. Kumar et al.⁴⁴ also observed that incorporating GNP resulted in a noticeable rise in thrust force, accompanied by an increase in delamination.

Referring to the NFS analysis in section 4.2.1, the impact of the layup structure on delamination status aligns with the ultrasonic option, as also depicted in [Figure 12\(e\)](#). The delamination values in [Figure 17\(a\)](#) and [\(b\)](#) demonstrate that employing a symmetric arrangement slightly reduced delamination compared to an asymmetric layout. Tabatabaeian et al.²⁹ observed that delamination damage tends to be more pronounced when an unsymmetrical layup arrangement is used. This reduction can be attributed to the lower thermal expansion coefficient between layers in a symmetrical layup, diminishing residual stress during curing and cooling processes. Since delamination is linked to residual stress,^{81–83} symmetrical lay-up specimens experience reduced occurrences. The curved nature of asymmetric specimens makes them prone to delamination due to bending, while the flat geometry of symmetric ones acts as a protective measure. [Figure 17\(c\)](#) visually compares the holes created in both lay-up configurations. Additionally, [Figure 17\(a\)](#) and [\(b\)](#) reveal that the drilled boundaries of

symmetric layup were noticeably smoother than their asymmetric counterparts. [Figure 17\(b\)](#) shows evident traces of material flaking-off, a characteristic less prominent in symmetric configurations.

Thrust force. The evaluation of thrust force contributes to longer tool lifespan and higher machining efficiency, facilitating the planning of CFRP machining processes.⁸⁴ The main effects plot in [Figure 18](#) depicts the impact of different control parameters on thrust force, clarifying their relationships and providing useful information about the contribution rate of each factor. The values of thrust force were obtained by computing the maximum value from the interpolated force-time diagrams, as illustrated in [Figure 19](#). The overall configuration of the plots suggests that the feed rate had the highest sensitivity to thrust force, while other factors show much lower impacts. This trend was previously confirmed by feature scoring analysis in section 4.2.2.

In [Figure 18\(a\)](#), it can be observed that the reduction in thrust force was achieved through the application of ultrasonics, as compared to non-ultrasonic drilling. This reduction was attributed to the intermittent impacts exerted on the CFRP sample during ultrasonic vibration, leading to increased fiber breakage within the material.⁸⁵ It is well established that higher thrust forces contribute to increased delamination during drilling, as the elevated mechanical stress tends to cause more damage around the hole. The use of ultrasonic-assisted drilling proves effective in reducing thrust force, which plays a key role in mitigating delamination. The ultrasonic vibrations enhance chip removal and reduce the load on the cutting edge, thereby decreasing the force required to penetrate the composite material. This reduction in mechanical stress at the drill-material interface leads to less pronounced delamination. The observed relationship between lower thrust forces and reduced delamination highlights the importance of controlling thrust force—particularly through ultrasonic assistance—in minimizing delamination in CFRP drilling. The impact of the tool type on thrust force is demonstrated in [Figure 18\(b\)](#), where the use of HSS drills containing cobalt resulted in reduced thrust force. This reduction can be attributed to the higher feed rates associated with the presence of cobalt in

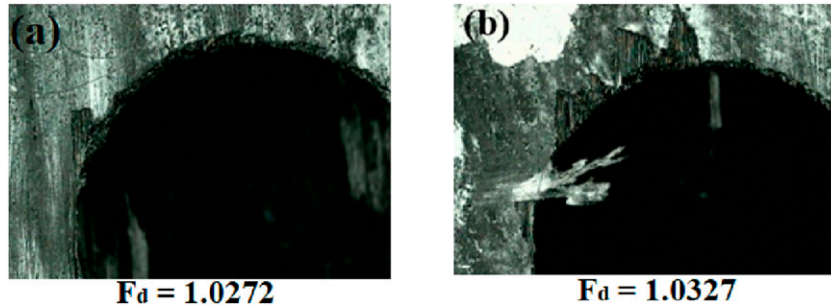


Figure 16. Illustration of the drilled holes with different materials: (a) CFRP, (b) CFRP/GNP.

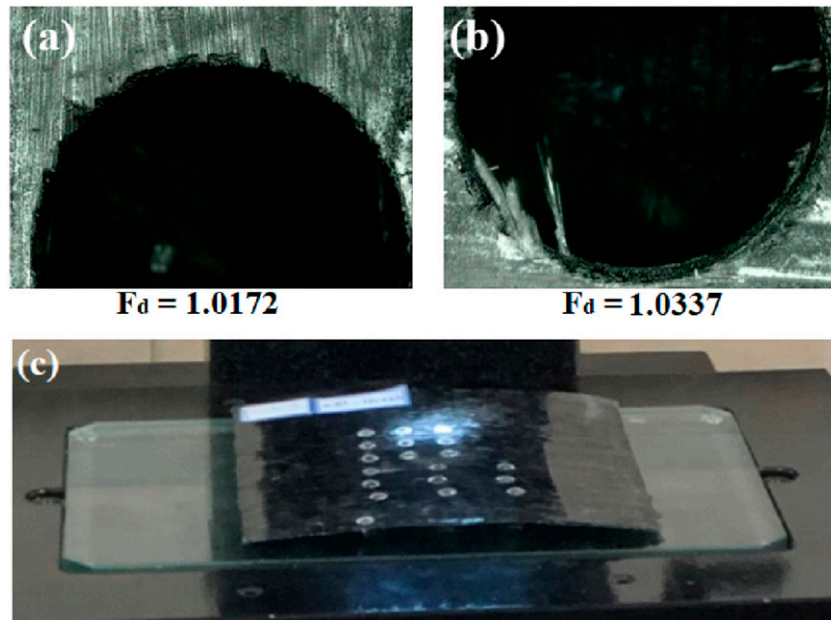


Figure 17. Illustration of CFRP drilled holes with different layups: (a) symmetrical, (b) asymmetrical, and (c) curved configuration of samples with an asymmetrical lay-up.

the cutting tool, which enhances heat resistance and contributes to improved performance. Figure 18(c) illustrates a substantial increase in thrust force at elevated feed rates, attributed to two primary factors. First, an augmented feed rate leads to greater cutting depth and larger material removal rate per revolution, subjecting the tool to higher forces during drilling.⁸⁶ Second, downward pressure is exerted by the tool on the CFRP for higher feed rates instead of cutting through the carbon fibers, amplifying the cutting force.

In Figure 18(d), the increase in thrust force from adding GNP to CFRP is evident. This is attributed to the greater strength of the CFRP/GNP hybrid nanocomposite compared to non-reinforced CFRP. Çelik et al.⁸⁷ previously reported similar findings, noting enhanced tensile strength in CFRP with GNP addition, as shown in the SEM images of Figure 7. The strong compatibility of GNP with carbon

fibers further boosts the composite overall strength, making it more difficult to machine. Figure 18(e) illustrates how the lay-up arrangement affects thrust force during drilling. A symmetrical lay-up reduces thrust force, as opposed to an asymmetric lay-up, which creates a curved shape due to differences in interlayer thermal expansion coefficients. This curvature increases cutting forces needed to drill asymmetric CFRP, as seen in Figure 17(c).

Limitations, challenges, and future scope

This study reveals key findings about predictive modeling of delamination and thrust force during CFRP composite drilling, but certain limitations must be acknowledged. A notable limitation is the relatively small dataset employed for training and testing the machine learning models, which may limit the generalizability of the findings. Although a

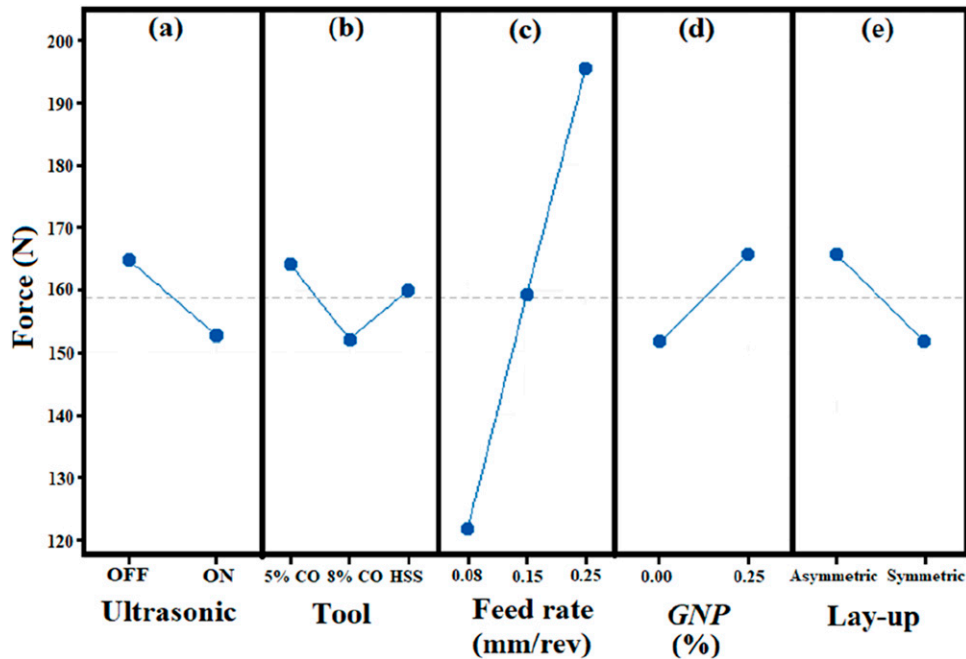


Figure 18. Main effects plots showing thrust force variation with respect to (a) ultrasonic activation, (b) tool type, (c) feed rate, (d) GNP content, and (e) lay-up configuration.

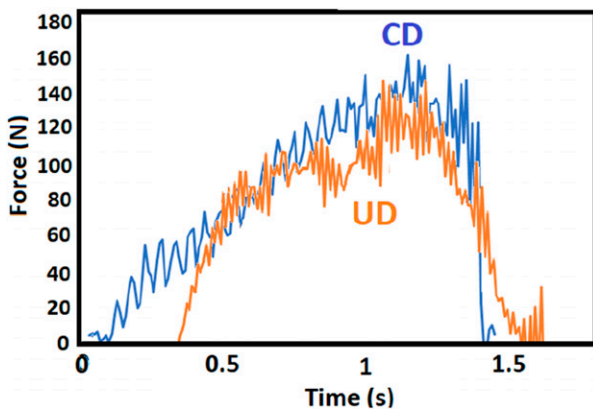


Figure 19. An exemplary diagram for determining the representative thrust force.

robust ensemble learning approach was used, the performance of the models could vary if tested on larger, more diverse datasets. Furthermore, the study primarily focused on specific machining parameters and material properties, omitting other factors such as environmental conditions, tool wear, and operator variability, all of which can influence drilling outcomes. Future research should explore the impact of these factors.

In addition, the study employed a nested feature scoring method to analyze feature importance, which, although useful, may not fully capture complex interactions between

variables. More advanced techniques for analyzing feature interactions would yield a more thorough analysis in future investigations. The stacked generalization approach used in this research did improve predictive accuracy, but its complexity may present challenges for practical implementation in industrial settings. Simplifying the model or offering clear guidelines for its use would enhance its applicability for practitioners.

Moreover, integrating real-time monitoring systems could further improve predictive accuracy by allowing dynamic adjustment of drilling parameters based on real-time data. The practical implications of this study are significant, as applying these findings could lead to improvements in drilling efficiency, reduction in material waste, and enhanced quality of CFRP components. These outcomes hold considerable potential for industries such as aerospace, where lightweight and durable materials are crucial, automotive, where high-performance parts are in demand, and wind energy, which requires resilient turbine blades. Addressing the limitations of this study while advancing predictive modeling methods could foster innovation and efficiency across these critical sectors.

Conclusion

The complexity of CFRP heterogeneous and anisotropic nature in drilling processes highlights the need for accurate predictive models. This study addressed this need

by using an advanced predictive modeling approach with ensemble ML and stacked generalization. The model aimed to link input factors such as material type, ultrasonic assistance, tooling type, stacking sequence, and feed rate with outcomes like delamination and thrust force. A Taguchi-based DoE was implemented, resulting in 72 data points from an orthogonal array. Various base learners were trained with optimized hyperparameters using grid search and Bayesian optimization. Four top-performing models were chosen from both non-ensemble and ensemble categories to enhance the ensemble effectiveness. The meta-model, constructed using stacked generalization with SGBR, was refined through iterative adjustments to improve robustness. Hyperparameters were further optimized using Bayesian techniques, leading to significant improvements in predictive accuracy. The ensemble approach notably reduced MAE and RMSE by approximately 97% and 124% for delamination, and 205% and 154% for thrust force compared to the best base learner, LGBR, demonstrating the effectiveness of the proposed ensemble method.

A novel NFS methodology was used to assess feature importance, combining rankings from SGBR, XGBoost, and RF for a thorough evaluation of primary and sub-features. Techniques such as one-hot encoding and normalization were applied to improve the analysis of feature significance, including categorical variables. The NFS evaluation revealed that tooling type and feed rate were the most critical factors affecting delamination and thrust force, respectively, while ultrasonic status had the least impact. The study also included visual and statistical analyses to explore variable-response interactions, comparing these insights with those from the NFS technique. Overall, this research advanced predictive modeling of CFRP drilling processes by employing a stacked ensemble learning strategy, resulting in a robust predictive model with extensive manufacturing applications.

The predictive methodology developed in this study offers significant industrial benefits by enhancing drilling efficiency, reducing material waste, and improving component quality in sectors reliant on CFRP composites. The advanced machine learning model, employing ensemble techniques and stacked generalization, optimizes drilling processes by accurately predicting thrust force and delamination. This leads to smoother operations, minimized tool wear, and better performance in high-stakes applications such as aerospace, automotive, and wind energy. The model provides practical guidance for tool selection and process optimization, and its adaptability supports diverse manufacturing contexts. Future enhancements, including real-time monitoring, could further refine the model, driving innovation and contributing to advancements in CFRP composite drilling technologies.

Acknowledgments

This is to certify that to the best of my knowledge; the content of this paper is my own work. This paper has not been submitted for any degree. I certify that the intellectual content of this paper is the product of our own work and that all the assistance received in preparing this paper and sources have been acknowledged.

Declaration of Conflicting Interests

The author(s) declared no potential conflicts of interest with respect to the research, authorship, and/or publication of this article.

Funding

The author(s) disclosed receipt of the following financial support for the research, authorship, and/or publication of this article: This work was supported by the Iran National Science Foundation (INSF) is gratefully acknowledged for financial support of this work (Project No. 99000063).

ORCID iDs

Mohammad Baraheni  <https://orcid.org/0000-0003-3500-0038>

Saeid Amini  <https://orcid.org/0000-0003-4650-707X>

Mohammad Fotouhi  <https://orcid.org/0000-0002-5956-4703>

Data availability statement

Data sharing not applicable to this article as no datasets were generated or analyzed during the current study.

References

1. Shokrian MD, Shelesh-Nezhad K and Soudmand BH. 3D FE analysis of tensile behavior for co-PP/SGF composite by considering interfacial debonding using CZM. *J Reinforc Plast Compos* 2016; 35: 365–374.
2. Kaveh A, Hashemi SB and Sheikholeslami R. Optimal design of laminated composite structures via hybrid charged system search and particle swarm optimization. *Asian Journal of Civil Engineering* 2013; 14(4): 587–604.
3. Shokrian MD, Shelesh-Nezhad K and H Soudmand B. Numerical simulation of a hybrid nanocomposite containing CaCO₃ and short glass fibers subjected to tensile loading. *Mechanics of Advanced Composite Structures* 2017; 4: 117–125.
4. Baraheni M, Hoseini AM and Najimi MR. Investigation on carbon fiber-reinforced polymer combined with graphene nanoparticles subjected to drilling operation using response surface methodology and non-dominated sorting genetic algorithm-II. *Proc IME E J Process Mech Eng*. 2024. DOI: [10.1177/09544089241230160](https://doi.org/10.1177/09544089241230160).
5. Tabatabaieian A, Baraheni M, Amini S, et al. Environmental, mechanical and materialistic effects on delamination damage of glass fiber composites: analysis and optimization. *J Compos Mater* 2019; 53: 3671–3680.

6. Baraheni M, Soudmand BH, Amini S, et al. Burr constitution analysis in ultrasonic-assisted drilling of CFRP/nano-graphene via experimental and data-driven methodologies. *J Reinforc Plast Compos*. 2024. DOI: [10.1177/07316844231225593](https://doi.org/10.1177/07316844231225593).
7. Baraheni M and Amini S. Influence of machining condition and nano-graphene incorporation on drilling load and hole quality in both conventional drilling and ultrasonic-assisted drilling of CFRP. *Arabian J Sci Eng* 2024; 49. DOI: [10.1007/s13369-024-08758-4](https://doi.org/10.1007/s13369-024-08758-4).
8. Raj SSR, Dhas JER and Jesuthanam CP. Challenges on machining characteristics of natural fiber-reinforced composites—A review. *J Reinforc Plast Compos* 2021; 40: 41–69.
9. Soudmand BH, Biglari H, Fotouhi M, et al. A finite element approach for addressing the interphase modulus and size interdependency and its integration into micromechanical elastic modulus prediction in polystyrene/SiO₂ nanocomposites. *Polymer* 2024; 309: 127463.
10. Mohsenzadeh R, Soudmand BH, Najafi A, et al. Morphology-Driven nanofiller size measurement integrated with micro-mechanical finite element analysis for quantifying interphase in polymer nanocomposites. *ACS Appl Mater Interfaces* 2024; 16: 39927–39941. DOI: [10.1021/acsami.4c02797](https://doi.org/10.1021/acsami.4c02797).
11. Soudmand BH and Mohsenzadeh R. Mechanical, morphological, and numerical evaluation of biocompatible ultra-high molecular weight polyethylene/nano-zeolite nanocomposites. *Polym Compos* 2024; 45: 3666–3682. DOI: [10.1002/pc.28018](https://doi.org/10.1002/pc.28018).
12. Mohsenzadeh R, Soudmand BH, Najafi AH, et al. Analysis of interfacial characteristics in polymer nanocomposites via visual particle recognition methodology and micro-mechanical predictive models. *Compos Sci Technol* 2024; 245: 110360.
13. Mohsenzadeh R, Soudmand BH and Shelesh-Nezhad K. Synergetic impacts of two rigid nano-scale inclusions on the mechanical and thermal performance of POM/carbon black/CaCO₃ ternary nanocomposite systems. *Polym Compos* 2022; 43(5): 3041–3056.
14. Mohsenzadeh R, Soudmand BH and Shelesh-Nezhad K. Failure analysis of POM ternary nanocomposites for gear applications: experimental and finite element study. *Eng Fail Anal* 2022; 140: 106606.
15. Mohsenzadeh R, Soudmand BH and Shelesh-Nezhad K. A combined experimental-numerical approach for life analysis and modeling of polymer-based ternary nanocomposite gears. *Tribol Int* 2022; 173: 107654.
16. Baraheni M, Shabgard MR, Amini S, et al. Experimental evaluation and optimization of parameters affecting delamination, geometrical tolerance and surface roughness in ultrasonic drilling of 3D-Printed PLA thermoplastic. *J Thermoplast Compos Mater*. 2024. DOI: [10.1177/08927057241264803](https://doi.org/10.1177/08927057241264803).
17. Kumar J, Abhishek K, Xu J, et al. Experimental investigation on machine-induced damages during the milling test of graphene/carbon incorporated thermoset polymer nanocomposites. *J Compos Sci* 2022; 6: 77.
18. Kumar J and Verma RK. A new criterion for drilling machinability evaluation of nanocomposites modified by graphene/carbon fiber epoxy matrix and optimization using combined compromise solution. *Surf Rev Lett* 2021; 28: 2150082. DOI: [10.1142/S0218625X21500827](https://doi.org/10.1142/S0218625X21500827).
19. Kumar J, Kesarwani S, Kharwar PK, et al. Mechanical performance and drilling machinability evaluation of carbon nano onions (CNOs) reinforced polymer nanocomposites. *Int J Interact Des Manuf* 2023; 17: 169–186. DOI: [10.1007/s12008-022-01160-0](https://doi.org/10.1007/s12008-022-01160-0).
20. Kumar K, Kumar J, Singh VK, et al. An integrated module for machinability evaluation and correlated response optimization during milling of carbon nanotube/glass fiber modified polymer composites. *Multiscale and Multidiscip Model Exp and Des* 2021; 4: 303–318. DOI: [10.1007/s41939-021-00099-1](https://doi.org/10.1007/s41939-021-00099-1).
21. Baraheni M, Shabgard MR and Amini S. Evaluating the hole quality produced by vibratory drilling: additive manufactured PLA+. *Int J Adv Manuf Technol* 2021; 117: 785–794.
22. Kumar D, Singh KK and Zitoune R. Experimental investigation of delamination and surface roughness in the drilling of GFRP composite material with different drills. *Adv Manuf Polym Compos Sci* 2016; 2: 47–56.
23. Kumar D and Singh KK. Investigation of delamination and surface quality of machined holes in drilling of multiwalled carbon nanotube doped epoxy/carbon fiber reinforced polymer nanocomposite. *Proc Inst Mech Eng Part L* 2019; 233: 647–663.
24. Abrao AM, Faria PE, Rubio JC, et al. Drilling of fiber reinforced plastics: a review. *J Mater Process Technol* 2007; 186: 1–7.
25. Dubey AD, Kumar J, Kyratsis P, et al. Stacking effect of carbon/glass fiber during drilling operation of laminated polymer composite. *Arch Metall Mater* 2024; 69: 589–598.
26. Kumar J and Verma RK. Delamination assessment during machining of laminated polymer nanocomposite. *International Journal of Modern Manufacturing Technologies (IJMMT)* 2021; 13.
27. Chen W-C. Some experimental investigations in the drilling of carbon fiber-reinforced plastic (CFRP) composite laminates. *Int J Mach Tool Manufact* 1997; 37: 1097–1108.
28. Faraz A, Biermann D and Weinert K. Cutting edge rounding: an innovative tool wear criterion in drilling CFRP composite laminates. *Int J Mach Tool Manufact* 2009; 49: 1185–1196.
29. Mehta M, Reinhart TJ and Soni AH. Effect of fastener hole drilling anomalies on structural integrity of PMR-15/Gr composite laminates. In: *Machining of composite materials (A 95-15178 02-37)*. Materials Park, OH: ASM International, 1992, pp. 113–126.
30. Davim JP, Rubio JC and Abrao AM. A novel approach based on digital image analysis to evaluate the delamination factor after drilling composite laminates. *Compos Sci Technol* 2007; 67: 1939–1945.

31. Tsao CC, Kuo KL and Hsu IC. Evaluation of a novel approach to a delamination factor after drilling composite laminates using a core-saw drill. *Int J Adv Manuf Technol* 2012; 59: 617–622. DOI: [10.1007/s00170-011-3532-y](https://doi.org/10.1007/s00170-011-3532-y).
32. Durão LMP, Tavares JMR, de Albuquerque VHC, et al. Damage evaluation of drilled carbon/epoxy laminates based on area assessment methods. *Compos Struct* 2013; 96: 576–583.
33. da Silva DNR. *Image processing methodology for assessment of drilling induced damage in CFRP*. Lisbon, Portugal: Universidade Nova de Lisboa, 2013.
34. Hocheng H and Tsao CC. The path towards delamination-free drilling of composite materials. *J Mater Process Technol* 2005; 167: 251–264.
35. Rahme P, Landon Y, Lachaud F, et al. Drilling of thick composite materials using a step gundrill. *Compos Appl Sci Manuf* 2017; 103: 304–313.
36. Rahmé P, Moussa P, Lachaud F, et al. Effect of adding a woven glass ply at the exit of the hole of CFRP laminates on delamination during drilling. *Composites Part A Applied Science and Manufacturing* 2020; 129: 105731.
37. Babu UH, Sai NV and Sahu RK. Artificial intelligence system approach for optimization of drilling parameters of glass-carbon fiber/polymer composites. *Silicon* 2021; 13: 2943–2957.
38. Kumar J, Verma RK and Mondal AK. Predictive modeling and machining performance optimization during drilling of polymer nanocomposites reinforced by graphene oxide/carbon fiber. *Arch Mech Eng* 2020; 67.
39. Behera RR, Ghadai RK, Kalita K, et al. Simultaneous prediction of delamination and surface roughness in drilling GFRP composite using ANN. *Int J Plast Technol* 2016; 20: 424–450.
40. Zhang Y and Xu X. Predicting thrust force during drilling of composite laminates with step drills through the Gaussian process regression. *Multidiscip Model Mater Struct* 2022; 18(5).
41. Kumar J, Singh RK and Xu J. Optimization of sustainable manufacturing processes: a case study during drilling of laminated nanocomposites. In: *Sustainable materials and manufacturing technologies*. Boca Raton, FL: CRC Press, 2023, pp. 29–43.
42. Kumar J and Verma RK. An integrated module for predictive modelling and machinability appraisal during milling of modified graphene/epoxy nanocomposites. *Aust J Mech Eng* 2023; 21: 682–694. DOI: [10.1080/14484846.2021.1913854](https://doi.org/10.1080/14484846.2021.1913854).
43. Kesarwani S, Pratap P, Kumar J, et al. An integrated approach for machining characteristics optimization of polymer nanocomposites. *Mater Today Proc* 2021; 44: 2638–2644.
44. Kumar J, Kumar Verma R and Debnath K. A new approach to control the delamination and thrust force during drilling of polymer nanocomposites reinforced by graphene oxide/carbon fiber. *Compos Struct* 2020; 253: 112786.
45. Vijayan D and Rajmohan T. Modeling and evolutionary computation on drilling of carbon fiber-reinforced polymer nanocomposite: an integrated approach using RSM based PSO. *J Braz Soc Mech Sci Eng* 2019; 41: 395–417.
46. Kumar J and Verma RK. Experimental investigation for machinability aspects of graphene oxide/carbon fiber reinforced polymer nanocomposites and predictive modeling using hybrid approach. *Defence Technology* 2021; 17: 1671–1686.
47. Kaybal HB, Ünüvar A, Koyunbakan M, et al. A novelty optimization approach for drilling of CFRP nanocomposite laminates. *Int J Adv Manuf Technol* 2019; 100: 2995–3012.
48. Shetty N, Herbert MA, Shetty R, et al. Soft computing techniques during drilling of bi-directional carbon fiber reinforced composite. *Appl Soft Comput* 2016; 41: 466–478.
49. Kumar Panchagnula K, Vamsi Krishna Jasti N and Sharma Panchagnula J. Prediction of drilling induced delamination and circularity deviation in GFRP nanocomposites using deep neural network. *Mater Today Proc* 2022; 62: 7118–7123.
50. Ge J, Zhang W, Luo M, et al. Multi-objective optimization of thermoplastic CF/PEKK drilling through a hybrid method: an approach towards sustainable manufacturing. *Compos Appl Sci Manuf* 2023; 167: 107418.
51. Soepangkat BOP, Norcahyo R, Effendi MK, et al. Multi-response optimization of carbon fiber reinforced polymer (CFRP) drilling using back propagation neural network-particle swarm optimization (BPNN-PSO). *Engineering Science and Technology, an International Journal* 2020; 23: 700–713.
52. Cui S, Yin Y, Wang D, et al. A stacking-based ensemble learning method for earthquake casualty prediction. *Appl Soft Comput* 2021; 101: 107038.
53. Galicia A, Talavera-Llames R, Troncoso A, et al. Multi-step forecasting for big data time series based on ensemble learning. *Knowl Base Syst* 2019; 163: 830–841.
54. Kang S, Kang P, Ko T, et al. An efficient and effective ensemble of support vector machines for anti-diabetic drug failure prediction. *Expert Syst Appl* 2015; 42: 4265–4273.
55. Koopialipoor M, Asteris PG, Salih Mohammed A, et al. Introducing stacking machine learning approaches for the prediction of rock deformation. *Transportation Geotechnics* 2022; 34: 100756.
56. Mendes-Moreira Ja., Soares C, Jorge AM, et al. Ensemble approaches for regression: a survey. *ACM Comput Surv* 2012; 45: 1–40.
57. Pavlyshenko B. Using stacking approaches for machine learning models. In: *2018 IEEE second international conference on data stream mining & processing (DSMP)*. Piscataway, NJ: IEEE, 2018, pp. 255–258.
58. Zounemat-Kermani M, Batelaan O, Fadaee M, et al. Ensemble machine learning paradigms in hydrology: a review. *J Hydrol* 2021; 598: 126266.
59. Nargis T, Shahabaz SM, Acharya S, et al. A comprehensive study on the optimization of drilling performance in hybrid nano-composites and neat CFRP composites using statistical and machine learning approaches. *Journal of Manufacturing and Materials Processing* 2024; 8: 67.

60. Guo N, Chen Y, Yan C, et al. Analysis and prediction of the influence of milling parameters on CFRP strength based on XGBoost algorithm. *J Braz Soc Mech Sci Eng* 2023; 45: 346. DOI: [10.1007/s40430-023-04267-x](https://doi.org/10.1007/s40430-023-04267-x).
61. Gupta P, Gupta N, Saxena KK, et al. A novel hybrid soft computing model using stacking with ensemble method for estimation of compressive strength of geopolymer composite. *Advances in Materials and Processing Technologies* 2022; 8: 1494–1509.
62. Aliha MRM, Kouchaki HG, Mohammadi MH, et al. Fracture toughness determination for epoxy-based polymer concrete mixtures: applicability of different rectangular beam and circular disc specimens. *Composites Part C: Open Access* 2024; 14: 100446.
63. Alexopoulos ND, Paragkaman Z, Poulin P, et al. Fracture related mechanical properties of low and high graphene reinforcement of epoxy nanocomposites. *Compos Sci Technol* 2017; 150: 194–204.
64. Babu J, Paul Alex N, Abraham SP, et al. Development of a comprehensive delamination assessment factor and its evaluation with high-speed drilling of composite laminates using a twist drill. *Proc IME B J Eng Manufact* 2018; 232: 2109–2121. DOI: [10.1177/0954405417690552](https://doi.org/10.1177/0954405417690552).
65. Babu J, Sunny T, Paul NA, et al. Assessment of delamination in composite materials: a review. *Proc IME B J Eng Manufact* 2016; 230: 1990–2003. DOI: [10.1177/0954405415619343](https://doi.org/10.1177/0954405415619343).
66. Alibrahim H and Ludwig SA. Hyperparameter optimization: comparing genetic algorithm against grid search and bayesian optimization. In: *2021 IEEE congress on evolutionary computation (CEC)*. Piscataway, NJ: IEEE, 2021, pp. 1551–1559.
67. Belete DM and Huchaiiah MD. Grid search in hyperparameter optimization of machine learning models for prediction of HIV/AIDS test results. *Int J Comput Appl* 2022; 44: 875–886.
68. Wu J, Chen X-Y, Zhang H, et al. Hyperparameter optimization for machine learning models based on Bayesian optimization. *Journal of Electronic Science and Technology* 2019; 17: 26–40.
69. Adler AI and Painsky A. Feature importance in gradient boosting trees with cross-validation feature selection. *Entropy* 2022; 24: 687.
70. Han J, Kim J, Park S, et al. Seismic vulnerability assessment and mapping of Gyeongju, South Korea using frequency ratio, decision tree, and random forest. *Sustainability* 2020; 12: 7787.
71. Li M, Zhou H, Zhang Y, et al. The effect of defects on the interfacial mechanical properties of graphene/epoxy composites. *RSC Adv* 2017; 7: 46101–46108.
72. Choubin B, Darabi H, Rahmati O, et al. River suspended sediment modelling using the CART model: a comparative study of machine learning techniques. *Sci Total Environ* 2018; 615: 272–281.
73. Godinho S, Guiomar N and Gil A. Using a stochastic gradient boosting algorithm to analyse the effectiveness of Landsat 8 data for montado land cover mapping: application in southern Portugal. *Int J Appl Earth Obs Geoinf* 2016; 49: 151–162.
74. Liang M, Chang Z, Wan Z, et al. Interpretable Ensemble-Machine-Learning models for predicting creep behavior of concrete. *Cement Concr Compos* 2022; 125: 104295.
75. Post A, Lin S, Waas AM, et al. Determining damage initiation of carbon fiber reinforced polymer composites using machine learning. *Polym Compos* 2023; 44: 932–953.
76. Cao S, Li HN, Huang W, et al. A delamination prediction model in ultrasonic vibration assisted drilling of CFRP composites. *J Mater Process Technol* 2022; 302: 117480.
77. Baraheni M and Amini S. Feasibility study of delamination in rotary ultrasonic-assisted drilling of glass fiber reinforced plastics. *J Reinforc Plast Compos* 2018; 37: 3–12.
78. Babu LS and Singh I. Studies on effect of drilling parameters on CFRP laminates using HSS, HSCO and solid carbide drills. *AIP Conf Proc* 2022; 2615.
79. Yaşar N and Günay M. The influences of varying feed rate on hole quality and force in drilling CFRP composite. *Gazi University Journal of Science* 2017; 30: 39–50.
80. Shyha IS, Aspinwall DK, Soo SL, et al. Drill geometry and operating effects when cutting small diameter holes in CFRP. *Int J Mach Tool Manufact* 2009; 49: 1008–1014.
81. Hussein R, Sadek A, Elbestawi MA, et al. Elimination of delamination and burr formation using high-frequency vibration-assisted drilling of hybrid CFRP/Ti6Al4V stacked material. *Int J Adv Manuf Technol* 2019; 105: 859–873.
82. Wu T, Degener S, Tinkloh S, et al. Characterization of residual stresses in fiber metal laminate interfaces—A combined approach applying hole-drilling method and energy-dispersive X-ray diffraction. *Compos Struct* 2022; 299: 116071.
83. Tabatabaeian A, Ghasemi AR, Shokrieh MM, et al. Residual stress in engineering materials: a review. *Adv Eng Mater* 2022; 24: 2100786.
84. Song Y, Cao H, Zheng W, et al. Cutting force modeling of machining carbon fiber reinforced polymer (CFRP) composites: a review. *Compos Struct* 2022; 299: 116096.
85. Amini S, Baraheni M and Mardiha A. Parametric investigation of rotary ultrasonic drilling of carbon fiber reinforced plastics. *Proc IME E J Process Mech Eng* 2018; 232: 540–554.
86. Qiu X, Li P, Niu Q, et al. Influence of machining parameters and tool structure on cutting force and hole wall damage in drilling CFRP with stepped drills. *Int J Adv Manuf Technol* 2018; 97: 857–865.
87. Çelik YH, Kilickap E and Koçyiğit N. Evaluation of drilling performances of nanocomposites reinforced with graphene and graphene oxide. *Int J Adv Manuf Technol* 2019; 100: 2371–2385.